Technical Report Documentation Page

1. Report No. FHWA/TX-0-1831-5	2. Government Accession No.	3. Recipient's Catalog No.
4. Title and Subtitle TRANSFORMED FIELD DOMAIN ANALYSIS OF PAVEMENTS SUBJECTED TO MOVING DYNAMIC TANDEM-AXLE LOADS AND INTEGRATING THEIR EFFECTS INTO THE CRCP-10 PROGRAM		5. Report Date August 2001
7. Author(s) Seong-Min Kim, Moon C. Won, and B. Frank McCullough		6. Performing Organization Code 8. Performing Organization Report No. Research Report 1831-5
9. Performing Organization Name and Address Center for Transportation Research The University of Texas at Austin 3208 Red River, Suite 200 Austin, TX 78705-2650		10. Work Unit No. (TRAIS) 11. Contract or Grant No. Project 0-1831
12. Sponsoring Agency Name and Address Texas Department of Transportation Research and Technology Implementation Office P.O. Box 5080 Austin, TX 78763-5080		13. Type of Report and Period Covered Research Report (9/00-8/01) 14. Sponsoring Agency Code

15. Supplementary Notes
Project conducted in co-operation with the U.S. Department of Transportation, Federal Highway Administration, and the Texas Department of Transportation.

16. Abstract

The dynamic displacement and stress responses of rigid and flexible pavements subjected to moving tandem-axle loads of constant amplitude and harmonic and arbitrary variations have been investigated. The pavement systems have been modeled using a plate of infinite extent on a viscoelastic foundation. Formulations have been developed in the transformed field domain using: (1) a double Fourier transform in space and moving space for moving loads of constant amplitude; (2) a triple Fourier transform in time, space, and moving space for moving loads of arbitrary variation; and (3) a double Fourier transform in space and moving space for the steady-state response to moving harmonic loads. The effects of viscous damping, vehicle speed, load frequency, and phase between front- and rear-axle loads have been investigated. The analysis results considering viscoelasticity show significant differences from those obtained with an elastic system. The pavement surface roughness causes dynamic variations in the load amplitude, and the maximum deflection and stress can significantly increase accordingly. The variation in the load amplitude and the differences in the phase angles between front- and rear-axle loads can make the maximum deflection and stress considerably larger. The use of tandem axle loads is necessary to find the accurate responses because the phase effect cannot be considered with single-axle loads. The formulations developed to find the wheel load stresses resulting from the moving tandem-axle loads have been integrated into CRCP-10, which is the updated computer program of CRCP-9.

17. Key Words Transformed field domain, Fourier transform, moving load, tandem axle, wheel load stress	18. Distribution Statement No restrictions. This document is available to the public through the National Technical Information Service, Springfield, Virginia 22161.

19. Security Classif. (of report) Unclassified	20. Security Classif. (of this page) Unclassified	21. No. of pages 74	22. Price

Form DOT F 1700.7 (8-72) Reproduction of completed page authorized

TRANSFORMED FIELD DOMAIN ANALYSIS OF PAVEMENTS SUBJECTED TO MOVING DYNAMIC TANDEM-AXLE LOADS AND INTEGRATING THEIR EFFECTS INTO THE CRCP-10 PROGRAM

by

Seong-Min Kim
Moon C. Won
B. Frank McCullough

Research Report No. 1831-5

Research Project 0-1831
Project Title: *Improvement of Concrete Pavement Performance Model*

Conducted for the

TEXAS DEPARTMENT OF TRANSPORTATION

in co-operation with the

U.S. DEPARTMENT OF TRANSPORTATION
Federal Highway Administration

by the

CENTER FOR TRANSPORTATION RESEARCH
Bureau of Engineering Research
THE UNIVERSITY OF TEXAS AT AUSTIN

August 2001

DISCLAIMERS

The contents of this report reflect the views of the authors, who are responsible for the facts and the accuracy of the data presented herein. The contents do not necessarily reflect the official views or policies of the Federal Highway Administration or the Texas Department of Transportation. This report does not constitute a standard, specification, or regulation.

There was no invention or discovery conceived or first actually reduced to practice in the course of or under this contract, including any art, method, process, machine, manufacture, design or composition of matter, or any new and useful improvement thereof, or any variety of plant, which is or may be patentable under the patent laws of the United States of America or any foreign country.

NOT INTENDED FOR CONSTRUCTION,
BIDDING, OR PERMIT PURPOSES

B. Frank McCullough, P.E. (Texas No. 19914)
Research Supervisor

ACKNOWLEDGMENTS

The researchers would like to acknowledge the expert assistance and guidance provided by the TxDOT project monitoring committee, which included G. Lantz (CSTC), G. Graham (CST-PAV), G. Lankes (CSTM), J. Kosel (CSTC), and Moon C. Won (CSTM).

Research performed in cooperation with the Texas Department of Transportation and the U.S. Department of Transportation, Federal Highway Administration.

TABLE OF CONTENTS

LIST OF FIGURES

LIST OF TABLES

CHAPTER 1. INTRODUCTION

1.1 BACKGROUND AND OBJECTIVE

State highway agencies are under constant public pressure to provide optimal pavement systems with limited resources. To ensure the effectiveness of their pavement management systems, it is important for those agencies to be able to predict the remaining life of a pavement with reasonable accuracy. For remaining pavement life or fatigue analyses, wheel load stresses and deflections have often been calculated using static load conditions (Refs 1, 2); however, critical wheel load stresses and deflections are induced by moving dynamic loads. A number of studies have recently been conducted to find the dynamic response of pavement systems to moving loads. Most of the studies have used moving loads with a constant amplitude (Refs 3, 4) and have not considered variations in amplitude with time that might result from the pavement surface roughness and the mechanical systems of the vehicles. The pavement response due to moving trucks also depends on the distance between axles as well as between wheels; however, most analyses have used single-axle or single-wheel load instead of tandem-axle and dual-wheel loads for simplicity of analysis.

The primary objective of this study was to examine and discuss the dynamic response of rigid and flexible pavements subjected to moving tandem-axle loads of constant amplitude and harmonic and arbitrary amplitude variations with a constant advance velocity. A plate on viscoelastic foundation was employed as a pavement model (Refs 2, 5, 6, 7). The viscoelastic nature of underlying layers was incorporated into the model as a viscoelastic foundation. The materials were assumed to be linear elastic and the plate was assumed to extend to infinity in the horizontal plane, so the effect of discontinuities in the pavement system at cracks, joints, and edges was ignored. The shape of the tire-pavement contact area was assumed to be rectangular, and any change in the shape during load variation was neglected. The load pressure within the contact area was assumed to be uniformly distributed. We developed formulations in the transformed field domain using: (1) a double Fourier transform in space and moving space for moving loads of constant amplitude; (2) a triple Fourier transform in time, space, and moving space for moving loads of arbitrary variation; and (3) a double Fourier transform in space and moving space for the steady-state response to moving harmonic loads. We investigated the effects of various parameters such as viscous damping, velocity, load frequency, and phase between front and rear axle loads on the pavement response.

Another objective of this study was to include the effect of the moving tandem-axle loads in the CRCP-9 computer program (Refs 8, 9, 10) using developed formulations. CRCP-9 and previous versions of the CRCP computer programs such as CRCP-8 (Ref 11) consider the wheel load effects by calculating wheel load stresses using Westergaard equations (Ref 1), which means that they consider only the static single-wheel load and do not include the moving dynamic tandem-axle loads. CRCP-10, the updated CRCP-9

computer program, has been developed to include the effect of the moving dynamic tandem-axle loads.

1.2 ORGANIZATION

This report consists of six chapters and an appendix. The background and objective of this study are presented in Chapter 1. Chapter 2 presents formulations to obtain the displacement and stress responses of the pavement systems subjected to moving dynamic tandem-axle loads. Using the developed formulations explained in Chapter 2, in Chapter 3 we investigate the stress response of the concrete pavements for various conditions of vehicle speed, viscous damping, load frequency, and phase between front- and rear-axle loads. Chapter 4 describes the flexible pavement response to moving tandem-axle loads. Because the flexible pavement performance is related to the vertical displacements that cause rutting and to the tensile stresses at the bottom of the surface (asphalt mixtures) layer that cause cracking, the displacements and tensile stresses at the bottom of the surface layer are investigated. The formulations developed to find the wheel load stresses that result from the moving tandem-axle loads are integrated into CRCP-10, which is the updated computer program of CRCP-9, and the details of the procedure are explained in Chapter 5. Finally, Chapter 6 includes our summary, conclusions, and recommendations. The subroutine program included in CRCP-10 to analyze the stresses of concrete pavements caused by the moving tandem-axle loads is listed in Appendix A.

CHAPTER 2. FORMULATIONS IN TRANSFORMED FIELD DOMAINS

2.1 FORMULATIONS FOR DISPLACEMENTS AND STRESSES

The dynamic displacement response of a plate of infinite extent on a viscoelastic foundation subjected to moving loads whose amplitudes change with time, shown in Figure 2.1, can be obtained using a triple Fourier transform in time, space, and moving space. The governing differential equation for the vertical displacements w in a fixed Cartesian coordinate system {x, y, z}, neglecting rotatory moments of inertia and shear deformation, can be written as

$$D_P\left(\frac{\partial^4 w(x,y,t)}{\partial x^4}+2\frac{\partial^4 w(x,y,t)}{\partial x^2\partial y^2}+\frac{\partial^4 w(x,y,t)}{\partial y^4}\right)+m\frac{\partial^2 w(x,y,t)}{\partial t^2} + c\frac{\partial w(x,y,t)}{\partial t}+kw(x,y,t)=q(x,y,t), \tag{2.1}$$

where D_P is the flexural rigidity of the plate defined by

$$D_P=\frac{Eh^3}{12(1-\nu^2)} \tag{2.2}$$

and m, k, and c are the mass of plate per unit of area, stiffness of foundation per unit of area, and viscous damping constant of foundation, respectively. E is the elastic modulus of the plate, h is the thickness of the plate, ν is Poisson's ratio of the plate, and q is the loading function.

Instead of obtaining the response at a fixed position, it would be more convenient to obtain the response at a moving position when the load amplitude varies and the critical response is of interest. If the loads are moving in the positive x direction with a constant advance velocity V, a moving coordinate η is defined by x-Vt. Eq. 2.1 can then be rewritten as

$$D_P\left(\frac{\partial^4 w(\eta,y,t)}{\partial \eta^4}+2\frac{\partial^4 w(\eta,y,t)}{\partial \eta^2\partial y^2}+\frac{\partial^4 w(\eta,y,t)}{\partial y^4}\right)+m\left(\frac{\partial^2 w(\eta,y,t)}{\partial t^2}-2V\frac{\partial^2 w(\eta,y,t)}{\partial t\partial \eta} + V^2\frac{\partial^2 w(\eta,y,t)}{\partial \eta^2}\right)+c\left(\frac{\partial w(\eta,y,t)}{\partial t}-V\frac{\partial w(\eta,y,t)}{\partial \eta}\right)+kw(\eta,y,t)=q(\eta,y,t) \tag{2.3}$$

If ξ, ζ, and Ω are assumed to be the transformed fields of η (moving space), y (fixed space), and t (time), and $w(\eta,y,t)$ and $q(\eta,y,t)$ are written in the form of

$W(\xi,\zeta,\Omega)e^{i\Omega t}e^{i\xi\eta}e^{i\zeta y}$ and $Q(\xi,\zeta,\Omega)e^{i\Omega t}e^{i\xi\eta}e^{i\zeta y}$, the transformed displacements $W(\xi,\zeta,\Omega)$ can be obtained by

$$W(\xi,\zeta,\Omega) = \frac{Q(\xi,\zeta,\Omega)}{D_P(\xi^2+\zeta^2)^2 + k - m(\Omega - V\xi)^2 + ic(\Omega - V\xi)} \quad , \tag{2.4}$$

where $i = \sqrt{-1}$ and the transformed load $Q(\xi,\zeta,\Omega)$ is obtained using the triple Fourier transform

$$Q(\xi,\zeta,\Omega) = \int_{-\infty}^{\infty}\int_{-\infty}^{\infty}\int_{-\infty}^{\infty} q(\eta,y,t)\ e^{-i\xi\eta}e^{-i\zeta y}e^{-i\Omega t}\ d\eta dy dt \tag{2.5}$$

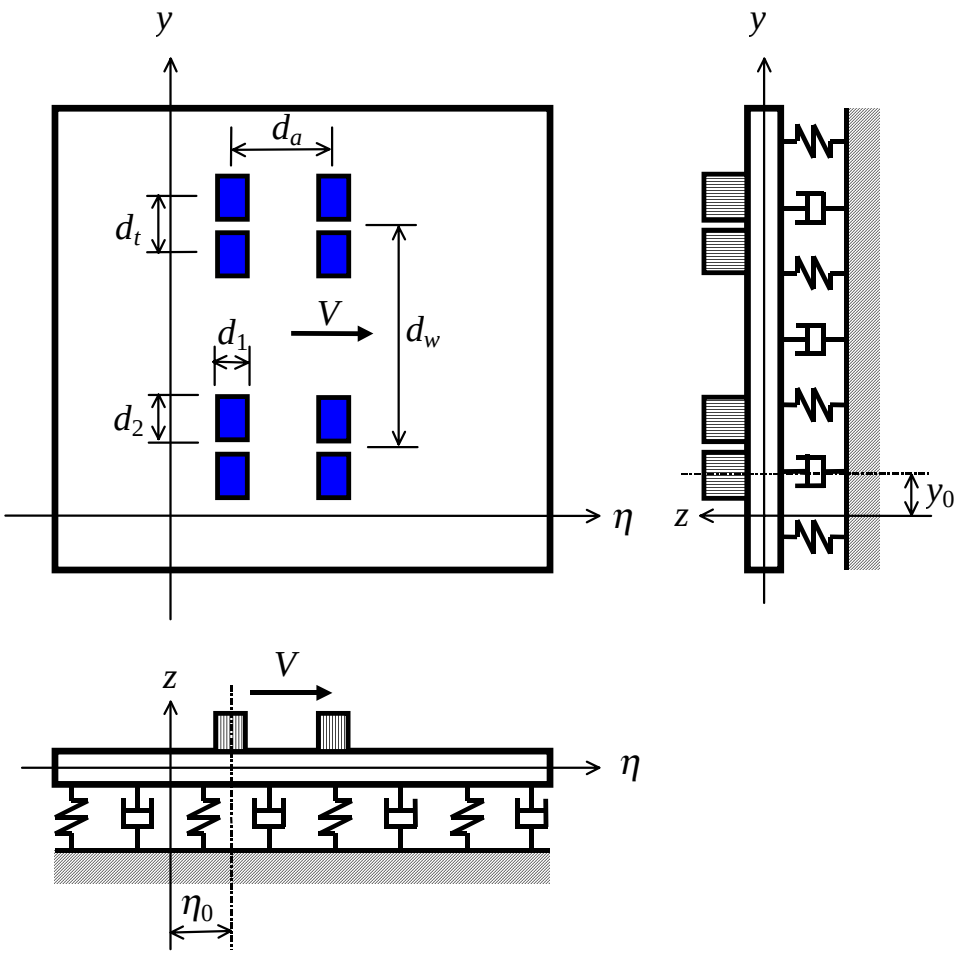

Figure 2.1. Plate on viscoelastic foundation with moving tandem-axle loads

Then, the dynamic displacement response can be obtained using the triple inverse Fourier transform

$$w(\eta, y, t) = \frac{1}{(2\pi)^3} \int_{-\infty}^{\infty} \int_{-\infty}^{\infty} \int_{-\infty}^{\infty} \frac{Q(\xi, \zeta, \Omega)}{D_P(\xi^2 + \zeta^2)^2 + k - m(\Omega - V\xi)^2 + ic(\Omega - V\xi)} \bullet e^{i\xi\eta} e^{i\zeta y} e^{i\Omega t} d\xi d\zeta d\Omega \quad (2.6)$$

Finally, the stresses in the moving space η and fixed space y can be obtained by

$$\sigma_\eta(\eta, y, t) = -\frac{Ez}{1-\nu^2}\left(\frac{\partial^2 w}{\partial \eta^2} + \nu \frac{\partial^2 w}{\partial y^2}\right) = \frac{Ez}{(1-\nu^2)(2\pi)^3}$$

$$\bullet \int_{-\infty}^{\infty} \int_{-\infty}^{\infty} \int_{-\infty}^{\infty} \frac{(\xi^2 + \nu\zeta^2) Q(\xi, \zeta, \Omega)}{D_P(\xi^2 + \zeta^2)^2 + k - m(\Omega - V\xi)^2 + ic(\Omega - V\xi)} e^{i\xi\eta} e^{i\zeta y} e^{i\Omega t} d\xi d\zeta d\Omega \quad (2.7)$$

$$\sigma_y(\eta, y, t) = -\frac{Ez}{1-\nu^2}\left(\frac{\partial^2 w}{\partial y^2} + \nu \frac{\partial^2 w}{\partial \eta^2}\right) = \frac{Ez}{(1-\nu^2)(2\pi)^3}$$

$$\bullet \int_{-\infty}^{\infty} \int_{-\infty}^{\infty} \int_{-\infty}^{\infty} \frac{(\nu\xi^2 + \zeta^2) Q(\xi, \zeta, \Omega)}{D_P(\xi^2 + \zeta^2)^2 + k - m(\Omega - V\xi)^2 + ic(\Omega - V\xi)} e^{i\xi\eta} e^{i\zeta y} e^{i\Omega t} d\xi d\zeta d\Omega \quad (2.8)$$

If frequency-independent linear hysteretic damping (or material damping) is considered in addition to viscous damping, an expression $2iDk$ can be used for the damping term, where D is the damping ratio (Refs 7, 12, 13). It should be noted that the sign of the linear hysteretic damping term needs to be consistent with that of the viscous damping term. In practice, the above equations are solved using the Fast Fourier Transform (FFT), which is a discrete transform. To successfully perform the FFT in the time and frequency domains, the system should have some damping. This requirement can be dropped when one uses the exponential window method (Refs 7, 14).

If the moving load has a harmonic variation of the amplitude $e^{i\bar{\Omega}t}$ and only the steady-state response is of interest, the displacement and stress responses in Eqs. 2.6 and 2.7 can be rewritten as

$$w(\eta, y, t) = \frac{1}{(2\pi)^2} \int_{-\infty}^{\infty} \int_{-\infty}^{\infty} \frac{Q(\xi, \zeta, t)}{D_P(\xi^2 + \zeta^2)^2 + k - m(\bar{\Omega} - V\xi)^2 + ic(\bar{\Omega} - V\xi)} e^{i\xi\eta} e^{i\zeta y} d\xi d\zeta \quad (2.9)$$

$$\sigma_\eta = \frac{Ez}{(1-\nu^2)(2\pi)^2} \int_{-\infty}^{\infty} \int_{-\infty}^{\infty} \frac{(\xi^2 + \nu\zeta^2) Q(\xi, \zeta, t)}{D_P(\xi^2 + \zeta^2)^2 + k - m(\bar{\Omega} - V\xi)^2 + ic(\bar{\Omega} - V\xi)} e^{i\xi\eta} e^{i\zeta y} d\xi d\zeta \quad (2.10)$$

with

$$Q(\xi,\zeta,t) = e^{i\overline{\Omega}t}\int_{-\infty}^{\infty}\int_{-\infty}^{\infty} q(\eta,y)\ e^{-i\xi\eta}e^{-i\zeta y}\ d\eta dy\,, \tag{2.11}$$

where $\overline{\Omega}$ is the load frequency. The stress in the fixed space σ_y can similarly be obtained. If the response to the force $\sin\overline{\Omega}t$ (the imaginary component of $e^{i\overline{\Omega}t}$) is considered, the imaginary component of Eqs. 2.9 and 2.10 should be used.

If the moving load with a constant amplitude ($\overline{\Omega} = 0$) is considered, Eqs. 2.9, 2.10, and 2.11 can be expressed as

$$w(\eta,y) = \frac{1}{(2\pi)^2}\int_{-\infty}^{\infty}\int_{-\infty}^{\infty}\frac{Q(\xi,\zeta)}{D_P(\xi^2+\zeta^2)^2 + k - mV^2\xi^2 - icV\xi}\ e^{i\xi\eta}e^{i\zeta y}d\xi d\zeta \tag{2.12}$$

$$\sigma_\eta = \frac{Ez}{(1-\nu^2)(2\pi)^2}\int_{-\infty}^{\infty}\int_{-\infty}^{\infty}\frac{(\xi^2+\nu\zeta^2)Q(\xi,\zeta)}{D_P(\xi^2+\zeta^2)^2 + k - mV^2\xi^2 - icV\xi}\ e^{i\xi\eta}e^{i\zeta y}d\xi d\zeta \tag{2.13}$$

with

$$Q(\xi,\zeta) = \int_{-\infty}^{\infty}\int_{-\infty}^{\infty} q(\eta,y)\ e^{-i\xi\eta}e^{-i\zeta y}\ d\eta dy \tag{2.14}$$

Because η is a point on the moving axis, the above equations represent the response at a moving point with time. The response at a fixed point can simply be obtained by using the relation $\eta = x\text{-}Vt$, where x is the fixed point.

2.2 FORMULATIONS FOR MOVING TANDEM-AXLE LOADS

The distance between front and rear tandem axles is large, and the critical pavement responses from a single tandem axle will not be affected by the other axle. Therefore, for the analysis in this study, a single tandem axle (a set of two axles) was selected. With the model shown in Figure 2.1, if the load pressure (load per unit of area) is q and η_0 and y_0 are the coordinates of the center of a load (in this study, it is the loaded area under the rear-axle right-wheel outside tire), each component of the transformed load Q defined in Eq. 2.14 for the rear axle can be obtained by

$$Q_1(\xi,\zeta) = \int_{\eta_0-\frac{d_1}{2}}^{\eta_0+\frac{d_1}{2}}\int_{y_0-\frac{d_2}{2}}^{y_0+\frac{d_2}{2}} qe^{-i\xi\eta}e^{-i\zeta y}dyd\eta = 4q\frac{\sin\frac{d_1\xi}{2}\sin\frac{d_2\zeta}{2}}{\xi\zeta}e^{-i\xi\eta_0}e^{-i\zeta y_0} \tag{2.15}$$

$$Q_2(\xi,\zeta)=\int_{\eta_0-\frac{d_1}{2}}^{\eta_0+\frac{d_1}{2}}\int_{y_0+d_t-\frac{d_2}{2}}^{y_0+d_t+\frac{d_2}{2}} qe^{-i\xi\eta}e^{-i\zeta y}dyd\eta=4q\frac{\sin\frac{d_1\xi}{2}\sin\frac{d_2\zeta}{2}}{\xi\zeta}e^{-i\xi\eta_0}e^{-i\zeta(y_0+d_t)} \tag{2.16}$$

$$Q_3(\xi,\zeta)=\int_{\eta_0-\frac{d_1}{2}}^{\eta_0+\frac{d_1}{2}}\int_{y_0+d_w-\frac{d_2}{2}}^{y_0+d_w+\frac{d_2}{2}} qe^{-i\xi\eta}e^{-i\zeta y}dyd\eta=4q\frac{\sin\frac{d_1\xi}{2}\sin\frac{d_2\zeta}{2}}{\xi\zeta}e^{-i\xi\eta_0}e^{-i\zeta(y_0+d_w)} \tag{2.17}$$

$$Q_4(\xi,\zeta)=\int_{\eta_0-\frac{d_1}{2}}^{\eta_0+\frac{d_1}{2}}\int_{y_0+d_t+d_w-\frac{d_2}{2}}^{y_0+d_t+d_w+\frac{d_2}{2}} qe^{-i\xi\eta}e^{-i\zeta y}dyd\eta=4q\frac{\sin\frac{d_1\xi}{2}\sin\frac{d_2\zeta}{2}}{\xi\zeta}e^{-i\xi\eta_0}e^{-i\zeta(y_0+d_t+d_w)}, \tag{2.18}$$

where d_1 and d_2 are the loaded lengths of a tire print in the η and y directions, respectively; d_t is the center-to-center distance between dual tires; and d_w is the distance between left and right wheels. The total transformed load for the rear axle can then be obtained by adding each component,

$$Q_{rear}(\xi,\zeta)=4q\frac{\sin\frac{d_1\xi}{2}\sin\frac{d_2\zeta}{2}}{\xi\zeta}e^{-i\xi\eta_0}e^{-i\zeta y_0}(1+e^{-i\zeta d_t}+e^{-i\zeta d_w}+e^{-i\zeta(d_t+d_w)}) \tag{2.19}$$

Similarly, each component of the transformed load for the front axle can be obtained by

$$Q_5(\xi,\zeta)=\int_{\eta_0+d_a-\frac{d_1}{2}}^{\eta_0+d_a+\frac{d_1}{2}}\int_{y_0-\frac{d_2}{2}}^{y_0+\frac{d_2}{2}} qe^{-i\xi\eta}e^{-i\zeta y}dyd\eta=4q\frac{\sin\frac{d_1\xi}{2}\sin\frac{d_2\zeta}{2}}{\xi\zeta}e^{-i\xi(\eta_0+d_a)}e^{-i\zeta y_0} \tag{2.20}$$

$$Q_6(\xi,\zeta)=\int_{\eta_0+d_a-\frac{d_1}{2}}^{\eta_0+d_a+\frac{d_1}{2}}\int_{y_0+d_t-\frac{d_2}{2}}^{y_0+d_t+\frac{d_2}{2}} qe^{-i\xi\eta}e^{-i\zeta y}dyd\eta=4q\frac{\sin\frac{d_1\xi}{2}\sin\frac{d_2\zeta}{2}}{\xi\zeta}e^{-i\xi(\eta_0+d_a)}e^{-i\zeta(y_0+d_t)} \tag{2.21}$$

$$Q_7(\xi,\zeta)=\int_{\eta_0+d_a-\frac{d_1}{2}}^{\eta_0+d_a+\frac{d_1}{2}}\int_{y_0+d_w-\frac{d_2}{2}}^{y_0+d_w+\frac{d_2}{2}} qe^{-i\xi\eta}e^{-i\zeta y}dyd\eta=4q\frac{\sin\frac{d_1\xi}{2}\sin\frac{d_2\zeta}{2}}{\xi\zeta}e^{-i\xi(\eta_0+d_a)}e^{-i\zeta(y_0+d_w)} \tag{2.22}$$

$$Q_8(\xi,\zeta)=\int_{\eta_0+d_a-\frac{d_1}{2}}^{\eta_0+d_a+\frac{d_1}{2}}\int_{y_0+d_t+d_w-\frac{d_2}{2}}^{y_0+d_t+d_w+\frac{d_2}{2}} qe^{-i\xi\eta}e^{-i\zeta y}dyd\eta=4q\frac{\sin\frac{d_1\xi}{2}\sin\frac{d_2\zeta}{2}}{\xi\zeta}e^{-i\xi(\eta_0+d_a)}e^{-i\zeta(y_0+d_t+d_w)}, \tag{2.23}$$

where d_a is the distance between front and rear axle tires. The total transformed load for the front axle can also be obtained by adding each component,

$$Q_{front}(\xi,\zeta) = 4q\frac{\sin\frac{d_1\xi}{2}\sin\frac{d_2\zeta}{2}}{\xi\zeta}e^{-i\xi(\eta_0+d_a)}e^{-i\zeta y_0}(1+e^{-i\zeta d_t}+e^{-i\zeta d_w}+e^{-i\zeta(d_t+d_w)}) \qquad (2.24)$$

Finally, the total transformed load Q for the tandem axle can be determined by adding Eqs. 2.19 and 2.24 as

$$Q(\xi,\zeta) = 4q\frac{\sin\frac{d_1\xi}{2}\sin\frac{d_2\zeta}{2}}{\xi\zeta}e^{-i\xi\eta_0}e^{-i\zeta y_0}(1+e^{-i\xi d_a})(1+e^{-i\zeta d_t}+e^{-i\zeta d_w}+e^{-i\zeta(d_t+d_w)}) \qquad (2.25)$$

If the harmonic variation of the load on each axle is $qe^{i\bar{\Omega}t}$ (four loaded areas in an axle have the same load history) and there is a phase φ between two axles, the transformed load defined in Eq. 2.11 can be given by

$$Q(\xi,\zeta,t) = 4q\frac{\sin\frac{d_1\xi}{2}\sin\frac{d_2\zeta}{2}}{\xi\zeta}e^{i\bar{\Omega}t}e^{-i\xi\eta_0}e^{-i\zeta y_0}(1+e^{i\varphi}e^{-i\xi d_a})(1+e^{-i\zeta d_t}+e^{-i\zeta d_w}+e^{-i\zeta(d_t+d_w)}) \qquad (2.26)$$

If the moving loads have arbitrary variations in amplitude and the variation is the same on each axle, the transformed load defined in Eq. 2.5 can be obtained by

$$Q(\xi,\zeta,\Omega) = 4\frac{\sin\frac{d_1\xi}{2}\sin\frac{d_2\zeta}{2}}{\xi\zeta}e^{-i\xi\eta_0}e^{-i\zeta y_0}(1+e^{-i\zeta d_t}+e^{-i\zeta d_w}+e^{-i\zeta(d_t+d_w)}) \bullet\int_{-\infty}^{\infty}(f_r(t)+e^{-i\xi d_a}f_f(t))\,e^{-i\Omega t}dt, \qquad (2.27)$$

where $f_r(t)$ and $f_f(t)$ are the variations in load amplitude with time on the rear- and front-axle tires.

An alternative way to obtain the response to moving multiple loads is to find the response to a moving load and superimpose the response according to the load distance. If a moving load has loaded lengths of d_1 and d_2 in the η and y directions and the load pressure (load per unit of area) is q, the transformed load Q defined in Eqs. 2.5, 2.11, and 2.14, can be obtained respectively by the equations

$$Q(\xi,\zeta,\Omega) = 4\frac{\sin\frac{d_1\xi}{2}\sin\frac{d_2\zeta}{2}}{\xi\zeta}e^{-i\xi\eta_0}e^{-i\zeta y_0}\int_{-\infty}^{\infty} f(t)e^{-i\Omega t}dt \tag{2.28}$$

$$Q(\xi,\zeta,t) = 4q\frac{\sin\frac{d_1\xi}{2}\sin\frac{d_2\zeta}{2}}{\xi\zeta}e^{i\overline{\Omega}t}e^{-i\xi\eta_0}e^{-i\zeta y_0} \tag{2.29}$$

$$Q(\xi,\zeta) = 4q\frac{\sin\frac{d_1\xi}{2}\sin\frac{d_2\zeta}{2}}{\xi\zeta}e^{-i\xi\eta_0}e^{-i\zeta y_0}, \tag{2.30}$$

where η_0 and y_0 are the coordinates of the center of the load and $f(t)$ is the variation in load amplitude with time.

To obtain the response to multiple loads, one can use the superposition method to consider the distances between the loads and superimpose each response. However, care should be taken in obtaining the steady-state response resulting from the moving harmonic loads because the amplitude of the response at each point does not occur at the same time. For instance, if there are two loads with center-to-center distances of L_η and L_y in the η and y directions, and the phase between the loads is φ, the steady-state response resulting from the load $\sin\overline{\Omega}t$ can be rewritten from Eqs. 2.9, 2.10, and 2.11 as

$$w(\eta,y,t) \text{ or } \sigma_\eta(\eta,y,t) = \sqrt{a(\eta,y)^2 + b(\eta,y)^2}\ \sin[\overline{\Omega}t + \arctan\frac{b(\eta,y)}{a(\eta,y)}] \tag{2.31}$$

with

$$a(\eta,y) + ib(\eta,y) = \frac{1}{(2\pi)^2}\int_{-\infty}^{\infty}\int_{-\infty}^{\infty}\frac{\int_{-\infty}^{\infty}\int_{-\infty}^{\infty} q(\eta,y)\ e^{-i\xi\eta}e^{-i\zeta y}d\eta dy}{D_P(\xi^2+\zeta^2)^2 + k - m(\overline{\Omega}-V\xi)^2 + ic(\overline{\Omega}-V\xi)}\ e^{i\xi\eta}e^{i\zeta y}d\xi d\zeta \tag{2.32}$$

for the displacements and with

$$a + ib = \frac{Ez}{(1-\nu^2)(2\pi)^2}\int_{-\infty}^{\infty}\int_{-\infty}^{\infty}\frac{(\xi^2+\nu\zeta^2)\int_{-\infty}^{\infty}\int_{-\infty}^{\infty} q(\eta,y)\ e^{-i\xi\eta}e^{-i\zeta y}d\eta dy}{D_P(\xi^2+\zeta^2)^2 + k - m(\overline{\Omega}-V\xi)^2 + ic(\overline{\Omega}-V\xi)}\ e^{i\xi\eta}e^{i\zeta y}d\xi d\zeta \tag{2.33}$$

for the stresses. The response to the other load $\sin(\overline{\Omega}t+\varphi)$ can be written as

$$\sqrt{a(\eta - L_\eta, y - L_y)^2 + b(\eta - L_\eta, y - L_y)^2}\ \sin[\overline{\Omega}t + \varphi + \arctan\frac{b(\eta - L_\eta, y - L_y)}{a(\eta - L_\eta, y - L_y)}] \quad (2.34)$$

Adding Eqs. 2.31 and 2.34, the amplitude of the response can be obtained as

$$\sqrt{a_1^{\,2} + b_1^{\,2} + a_2^{\,2} + b_2^{\,2} + 2[(a_1a_2 + b_1b_2)\cos\varphi - (a_1b_2 - b_1a_2)\sin\varphi]}\,, \quad (2.35)$$

where $a_1 = a(\eta, y)$, $b_1 = b(\eta, y)$, $a_2 = a(\eta - L_\eta, y - L_y)$, and $b_2 = b(\eta - L_\eta, y - L_y)$. If the two loads have constant amplitudes instead of harmonic variations, the response can be obtained simply by adding each response, $a(\eta, y) + a(\eta - L_\eta, y - L_y)$. For multiple loads such as dual-wheel single-axle loads and tandem-axle loads, the response can be obtained similarly using the above approach.

CHAPTER 3. RIGID PAVEMENT RESPONSE TO MOVING DYNAMIC TANDEM-AXLE LOADS

3.1 RESPONSE TO MOVING LOADS OF CONSTANT AMPLITUDE

We first investigated the concrete stress response that results from moving tandem-axle loads with a constant amplitude. The material properties and geometry of the concrete pavement model and the dimensions of the tandem-axle loads used in this study are listed in Table 3.1. Eqs. 2.13, 2.14, and 2.25 are used to obtain the analysis results for moving loads with a constant amplitude. For the FFT in the moving and fixed spaces and transformed field domains of those spaces, we used 2,048 for the number of transformed points and 1.27 cm (0.5 in.) for the distance increment.

Table 3.1. Material properties and load geometry for rigid pavement model

E	27,560 MPa (4,000 ksi)	d_1	17.78 cm (7 in.)
ν	0.15	d_2	20.32 cm (8 in.)
k	136 MN/m^3 (500 pci)	d_t	33 cm (13 in.)
h	30.48 cm (12 in.)	d_w	188 cm (74 in.)
m	708 kg/m^2 (0.00261 lb sec^2/in^3)	d_a	132 cm (52 in.)
D	0.5 %	c	12 MPa sec/m (44.24 lb sec/in^3)
Axle load	-80 kN (-18 kip)		

Figure 3.1(*a*) shows the effect of velocity (vehicle speed) on the maximum longitudinal tensile stress in concrete slabs for various viscous damping values. The logical values of the velocities up to 150 km/h (95 mph) are used in this study. If the system has no viscous damping, the maximum stress remains almost constant regardless of the velocity. If there is viscous damping, the maximum stress initially increases slightly and then decreases as the velocity becomes larger. As the viscous damping constant increases, the stress decreases significantly. It should be noted that the viscous damping constant depends largely on the types and moisture contents of underlying layers such as base, sub-base, and subgrade. Figure 3.1(*b*) shows the effect of velocity on the maximum transverse stress. The overall trend stays the same as those for the longitudinal stresses, except that the magnitude of the transverse stress is smaller than that of the longitudinal stress. Because the fatigue cracking potential of the concrete slab (critical stress) is the major focus of this study, only the longitudinal stresses are considered in the rest of this chapter. Note that the maximum stress can be either tensile or compressive because the neutral surface is at the mid-depth of the concrete slab. The maximum tensile and compressive stresses occur simultaneously at the

bottom and surface of the slab, respectively, at a point under the loads, which depends on the material properties, pavement structures, and load configurations. For a configuration shown in Figure 2.1, the maximum stress generally occurs at the rear axle and 28 cm (11 in.) inside from the center of the outside tire (in Figure 2.1, at the coordinate $\{\eta_0, y_0 + 28 \text{ cm}\}$). It does not always occur here, but varies slightly depending on viscous damping and velocity.

(a)

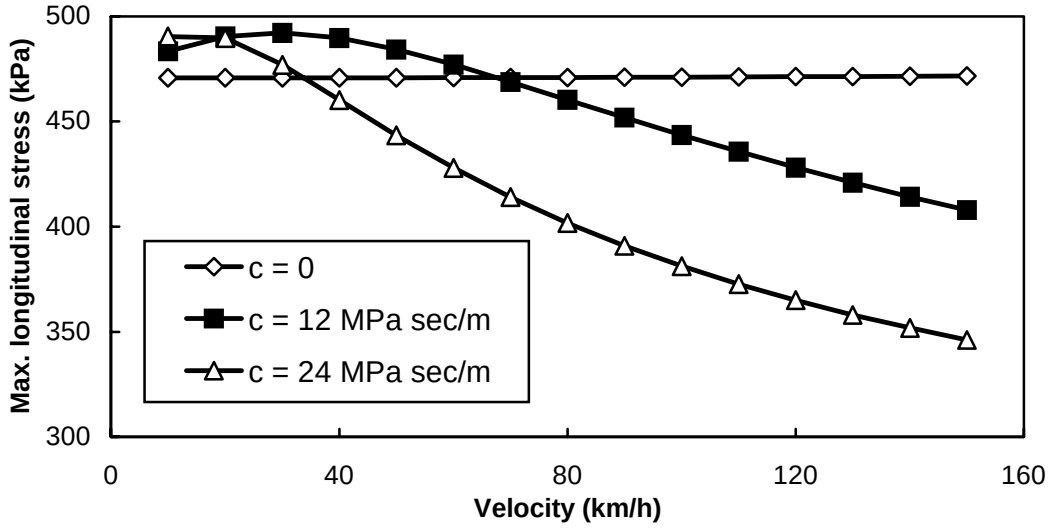

(b)

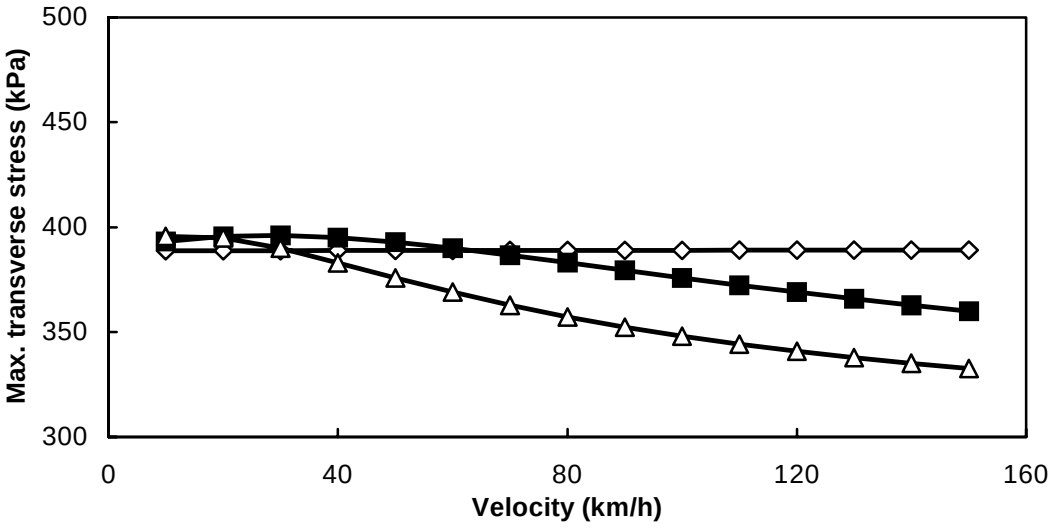

Figure 3.1. Effect of velocity for various viscous damping values: (a) on maximum longitudinal stress; (b) on maximum transverse stress (1 kPa = 0.145 psi, 1 km/h = 0.63 mph, 1 MPa sec/m = 3.69 psi sec/in.)

If the concrete slab is sufficiently large and the velocity is constant, the stress distribution under the moving loads is the same at any instant. This means that the stress distribution is moving with the loads. Figure 3.2 shows the longitudinal stress distribution along the moving coordinate near the loads at the *y* coordinate of y_0 + 28 cm where the maximum stress occurs. In the figure, the 0 distance represents the midpoint between the two axles. The figure shows the stress distribution for different viscous damping constants when a velocity is 40 km/h (25 mph). If there is no viscous damping, the stress distribution is symmetric with respect to the midpoint between the two axles. If there is viscous damping, the stress distribution is no longer symmetric. The peak stress under the front axle decreases, and the maximum stress occurs under the rear axle. Note that because the material damping (linear hysteretic damping) of the system in this study is very small (D = 0.5%), the stress distribution is essentially symmetric when there is no viscous damping. However, if material damping is large, the response is not symmetric even when there is no viscous damping (Refs 7, 13).

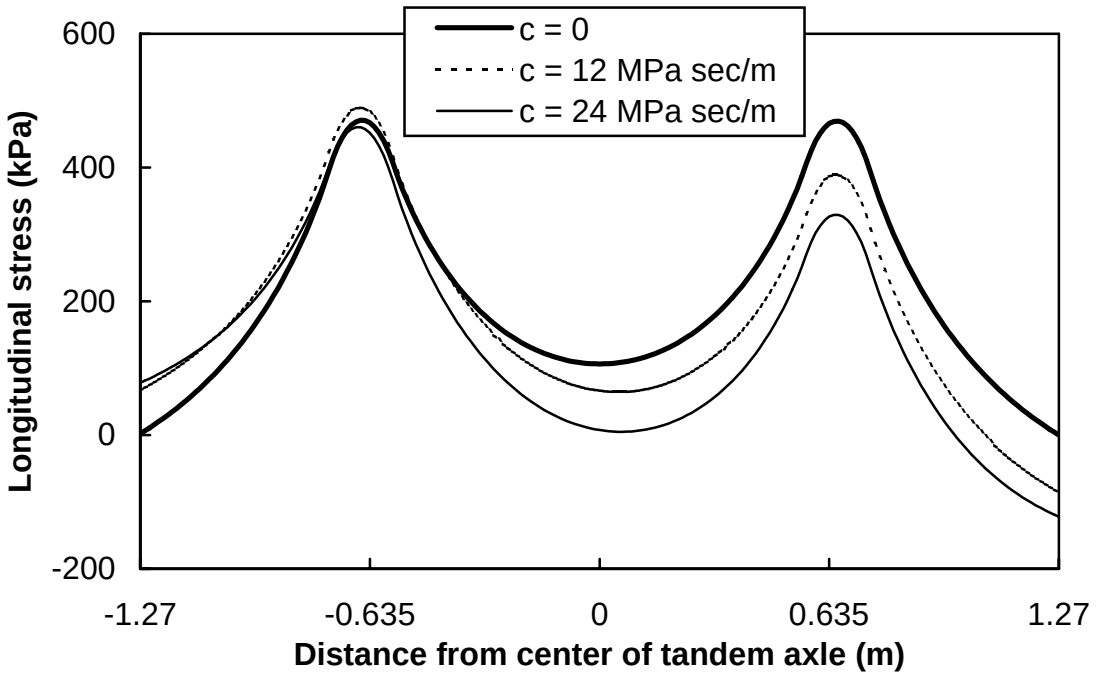

Figure 3.2. Longitudinal stress distribution for various viscous damping constants (1 kPa = 0.145 psi, 1 m = 3.28 ft, 1 MPa sec/m = 3.69 psi sec/in.)

The longitudinal stress distribution for various velocities with constant viscous damping of 12 MPa sec/m (44 psi sec/in.) is shown in Figure 3.3. The shapes of the stress distributions are very similar to one another regardless of the velocity, but the stresses decrease as the velocity increases.

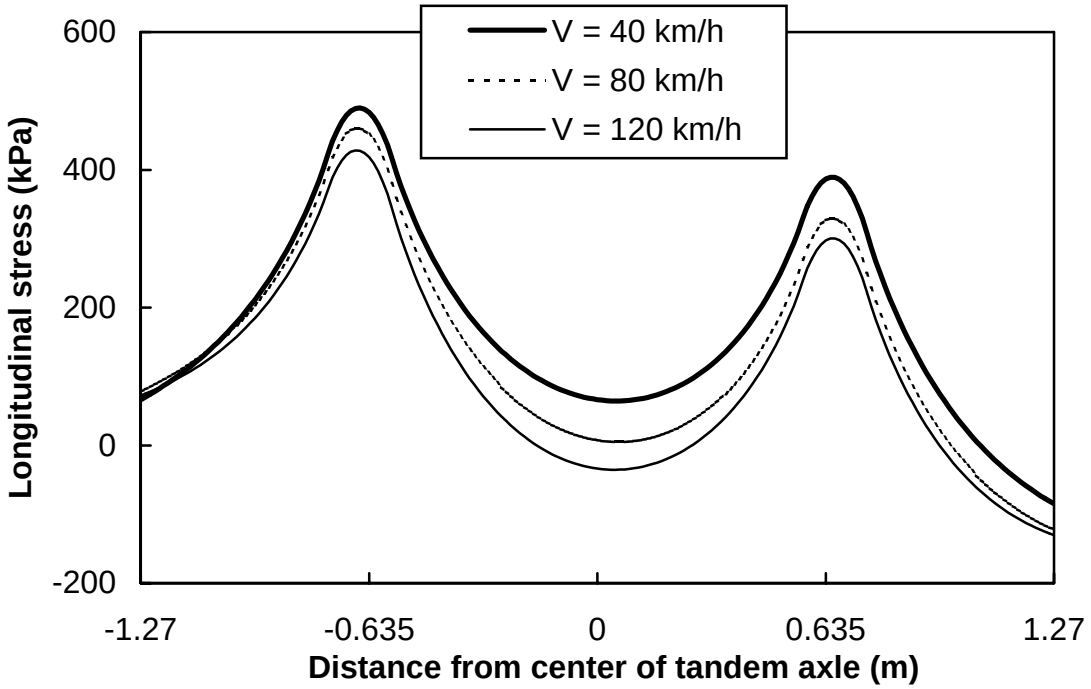

Figure 3.3. Longitudinal stress distribution for various load velocities (1 kPa = 0.145 psi, 1 m = 3.28 ft, 1 km/h = 0.63 mph)

3.2 RESPONSE TO MOVING ARBITRARY LOADS

The roughness of the pavement surface will cause a variation in load amplitude when a truck is moving. The stress response that results from this arbitrary variation of the load has been investigated. Eqs. 2.5, 2.7, and 2.27 are used to calculate stresses. To obtain the time histories of the dynamic loads on the front- and rear-axle tires, we used a computer program developed to predict the wheel loads in the Texas Mobile Load Simulator (TxMLS) research project with three different pavement profiles (Refs 15, 16). One is a perfectly smooth profile (ideal profile), and the others are profiles corresponding to present serviceability index (PSI) values of 4.5 and 2.0. Figure 3.4 shows the dynamic loads caused by various pavement roughnesses under the wheels of the front and rear axles when the velocity is 32 km/h (20 mph). As the pavement roughness increases, the load amplitude as well as its variation becomes larger. The maximum load amplitudes are about 10 percent and 40 percent larger on the pavements with PSI 4.5 and 2.5, respectively, than the load on the perfectly smooth pavement.

(a)

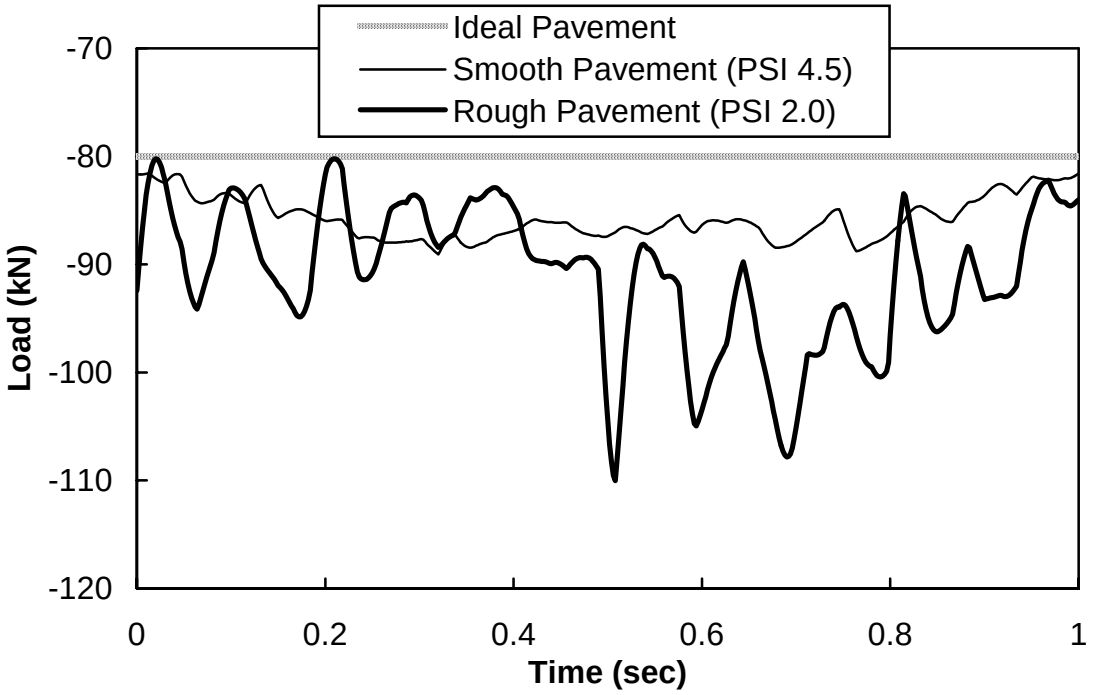

(b)

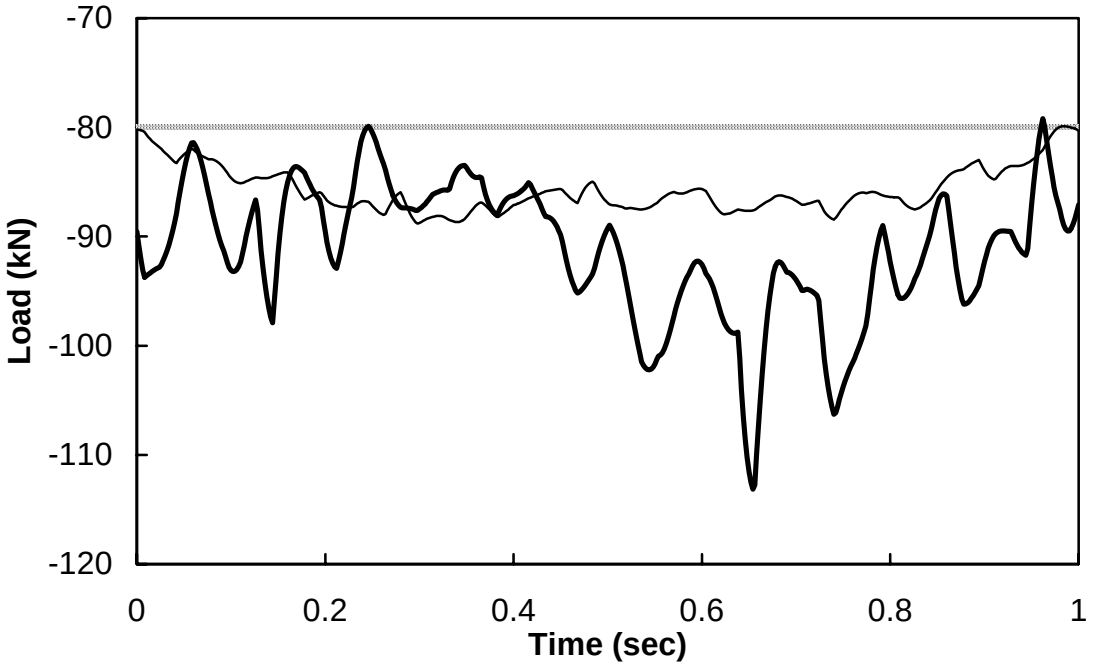

Figure 3.4. Time history of load for various pavement surface roughnesses: (a) on front-axle tires; (b) on rear-axle tires (1 kN = 0.225 kip)

The time histories of the longitudinal stresses under the front- and rear-axle tires at the coordinates of $\{\eta_0 + 132 \text{ cm}, y_0 + 28 \text{ cm}\}$ and $\{\eta_0, y_0 + 28 \text{ cm}\}$ are shown in Figures 3.5 and 3.6, respectively. The shapes of the stress time histories are very similar to those of the load time histories. The stresses under the rear-axle tires are larger than those under the front-axle tires. For the perfectly smooth pavement, the stress under the rear-axle tires is about 20 percent larger than that under the front-axle tires, even though the load applied is of the same magnitude. This trend of stresses larger under the rear-axle wheels than the front holds true for all roughnesses. Figure 3.6 shows that pavement roughness has a significant effect on the wheel load stress under the rear axle wheels, with 40% and 10% higher compared with the perfectly smooth surface for PSIs of 2.0 and 4.5, respectively. This analysis shows a significant effect of pavement roughness on wheel load stress and the subsequent fatigue life of pavements. The analysis supports the specification changes state highway agencies have been making to improve pavement smoothness.

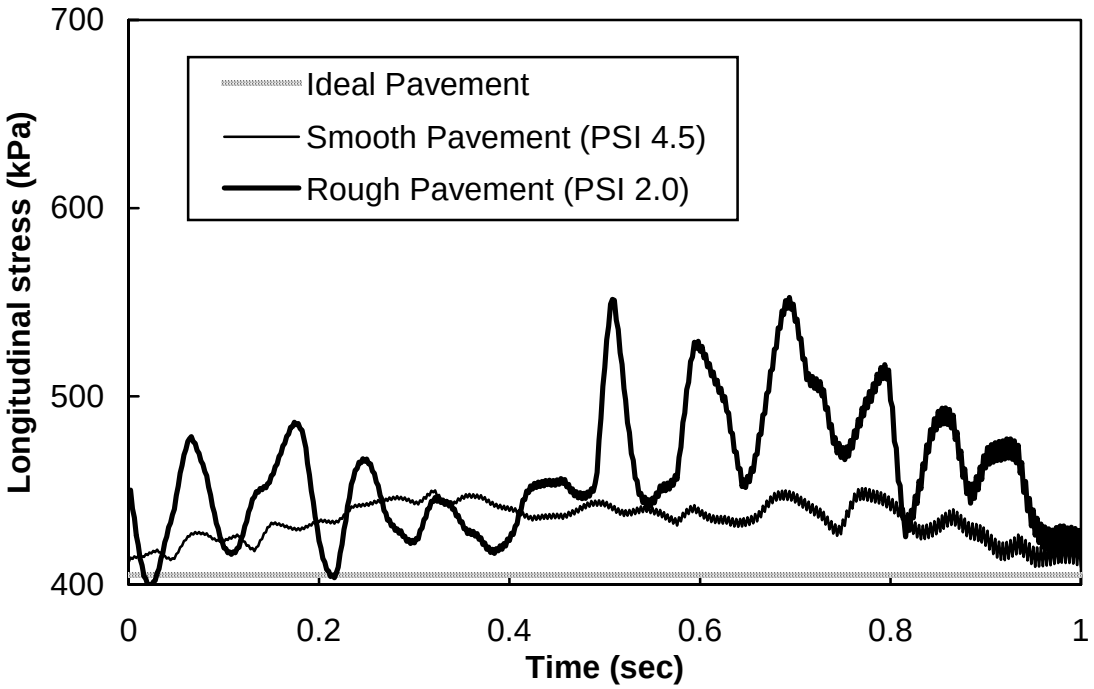

Figure 3.5. Time history of stress for various pavement surface roughnesses under front-axle tires (1 kPa = 0.145 psi)

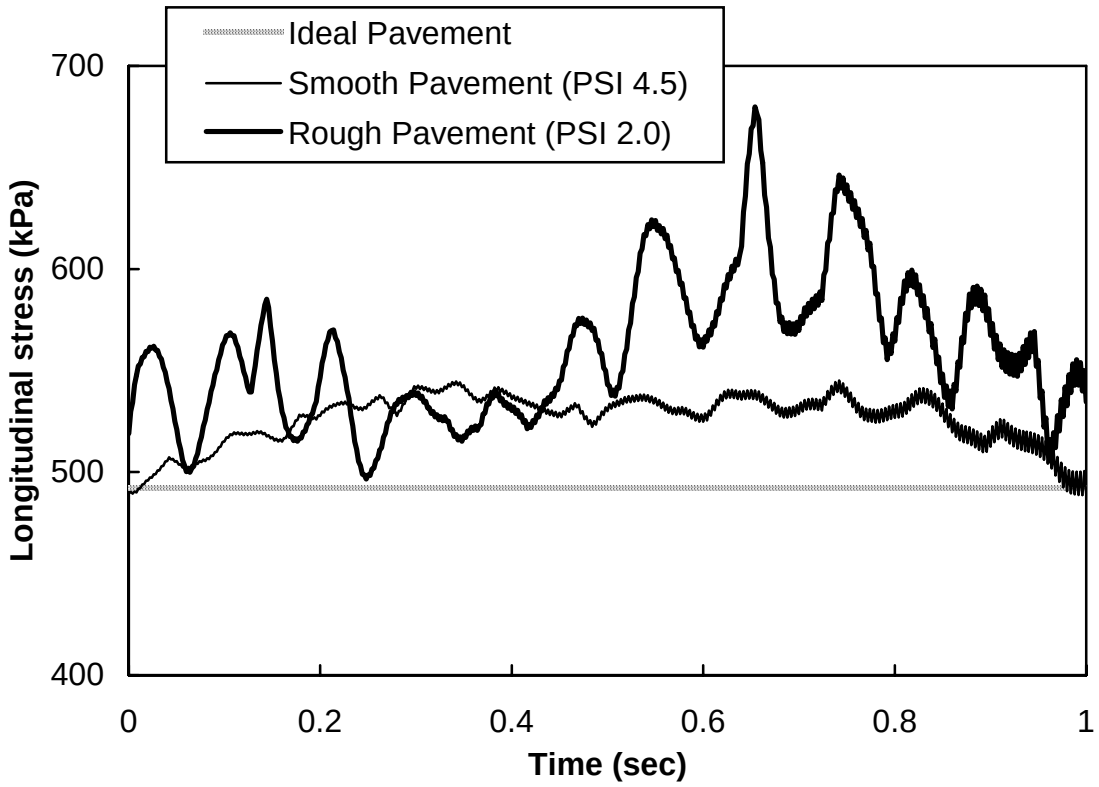

Figure 3.6. Time history of stress for various pavement surface roughnesses under rear-axle tires (1 kPa = 0.145 psi)

3.3 RESPONSE TO MOVING HARMONIC LOADS

A further investigation to evaluate the effect of load variation on the wheel load stresses has been conducted with the moving loads that consist of a constant amplitude component and a harmonic variation component. Eqs. 2.10, 2.11, and 2.26 are used to obtain the stresses subjected to moving harmonic loads. Figure 3.7(*a*) shows the constant amplitude of the load, harmonic variations under the front- and rear-axle tires, and combined loads. It is assumed that the phase between the front- and rear-axle loads is 180 degrees and the half amplitude of the harmonic load is 30 percent of the amplitude of the constant load. The stress distributions under the combined loads and their components of constant and harmonic loads are shown in Figure 3.7(*b*). Because the stress distribution under the moving harmonic loads changes with time, the maximum stresses along the moving coordinate are shown in the figure. Therefore, the combined stress distribution represents the maximum combined stress at each position and does not necessarily occur at the same time.

(a)

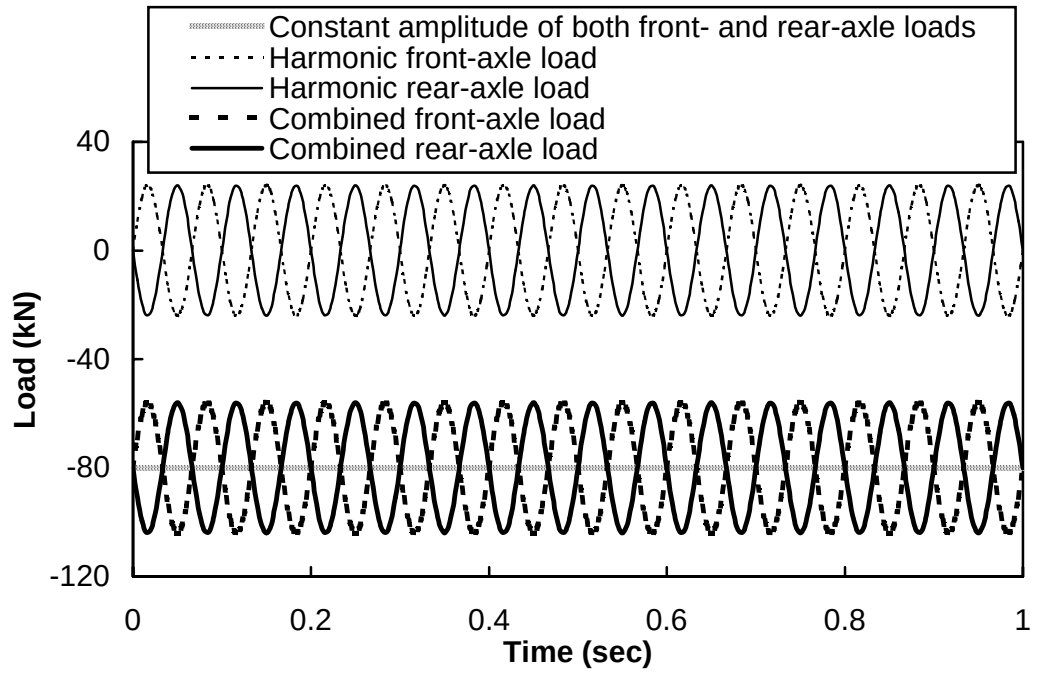

(b)

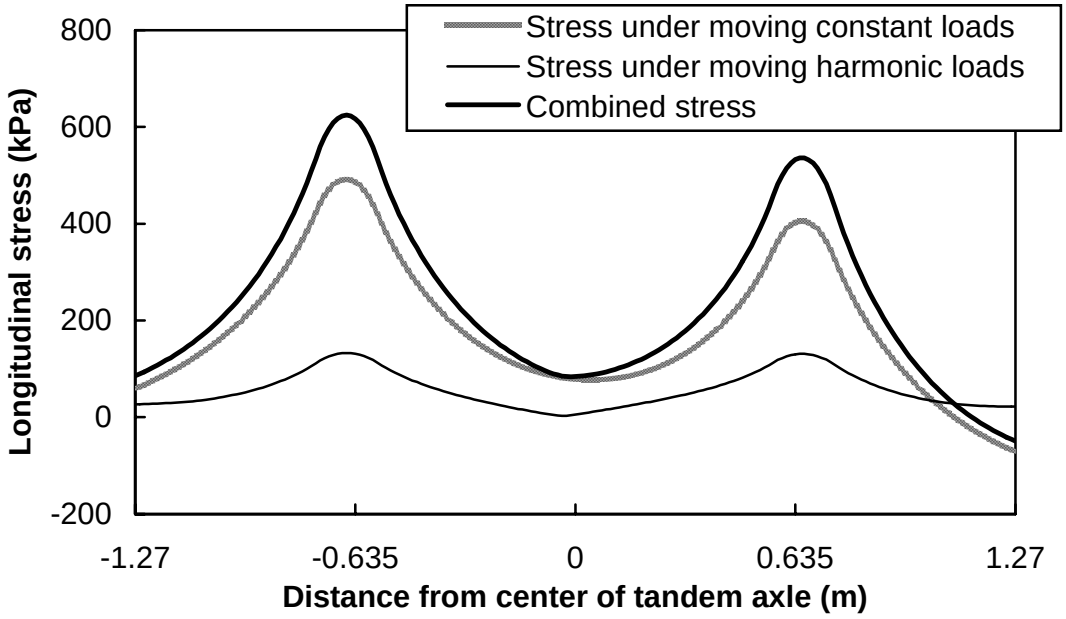

Figure 3.7. Combined load time history and stress distribution: (a) time histories of constant amplitude, harmonic, and combined loads on front and rear axles; (b) stress distributions under constant amplitude, harmonic, and combined loads (1 kN = 0.225 kip, 1 kPa = 0.145 psi, 1 m = 3.28 ft)

Figure 3.8 shows the effect of load frequency on the maximum stress. When there is no viscous damping, shown in Figures 3.8(*a*) and (*b*), the maximum stress increases slightly with increasing frequency. On the other hand, when viscous damping is considered with no phase between the front- and rear-axle loads, shown in Figure 3.8(*c*), the maximum stress decreases as the frequency increases. The significant stress decrease can be observed within the frequency of less than 10 Hz. If there is a phase of 180 degrees between the two axle loads, shown in Figure 3.8(*d*), the maximum stress decreases with increasing load frequency for a low velocity (40 km/h). As the velocity becomes higher, the maximum stress increases initially and decreases as the frequency becomes larger. Figure 3.9 shows velocity's effect on the maximum stress. With no viscous damping, velocity has little effect on the maximum stress, as shown in Figures 3.9(*a*) and (*b*). When viscous damping is considered, as shown in Figures 3.9(*c*) and (*d*), the maximum stress remains almost constant at velocities less than 40 km/h; however, it decreases as the velocity increases over that velocity. The effect of the phase between the front- and rear-axle loads on the maximum stress is shown in Figure 3.10. The maximum stress increases as the phase becomes close to 180 degrees (π radians), and then it decreases. The differences of about 5 to 8 percent between the maximum stresses for phase angles of 0 and 180 degrees are observed in this case. Therefore, a phase difference between the loads can increase the maximum stress.

As discussed above, variations in moving load characteristics such as amplitude, frequency, and phase can affect the stress significantly. We also have studied the stress response of concrete pavements subjected to moving pure harmonic loads with various frequencies and phases. Figure 3.11 shows the maximum stress distribution along the moving coordinate when there is no viscous damping. The maximum stress distribution is not much affected by the load frequency. When there is no phase, shown in Figure 3.11(*a*), the trend of the stress distribution is similar to that under the moving loads of constant amplitude (see Figure 3.2). On the other hand, with a phase angle of 180 degrees (Figure 3.11(*b*)), the maximum stress increases by about 23 percent. The stress at the midpoint of the tandem axle is 0 because the stress caused by the front- and rear-axle loads is of the same magnitude but with opposite signs. If there is viscous damping, the stress distribution is affected significantly by the load frequency, as shown in Figure 3.12. The maximum stress decreases as the load frequency increases. The difference between the maximum stresses for phase angles of 0 and 180 degrees is about 30 to 40 percent for a given frequency. At the midpoint of the tandem axle, the stress is no longer 0 for a phase angle of 180 degrees, as shown in Figure 3.12(*b*), because of the different magnitude of stress caused by the front and rear axles that result from damping. The effect of velocity can be observed in Figure 3.13. The velocity has little effect on the stresses, and the peak stresses under the front- and rear-axle loads are similar, which is different from those under the moving loads of constant amplitude (compare with Figure 3.3). Figure 3.14 shows the effect of phase angle between the front- and rear-axle loads. As the phase increases, the maximum stress becomes larger. The maximum stress difference between phase angles of 0 and 180 degrees is about 25 to 40 percent. This phase effect is significant and should be included in wheel-load stress analysis. Because the phase effect cannot be obtained with single-axle loads, the use of tandem-axle loads is needed.

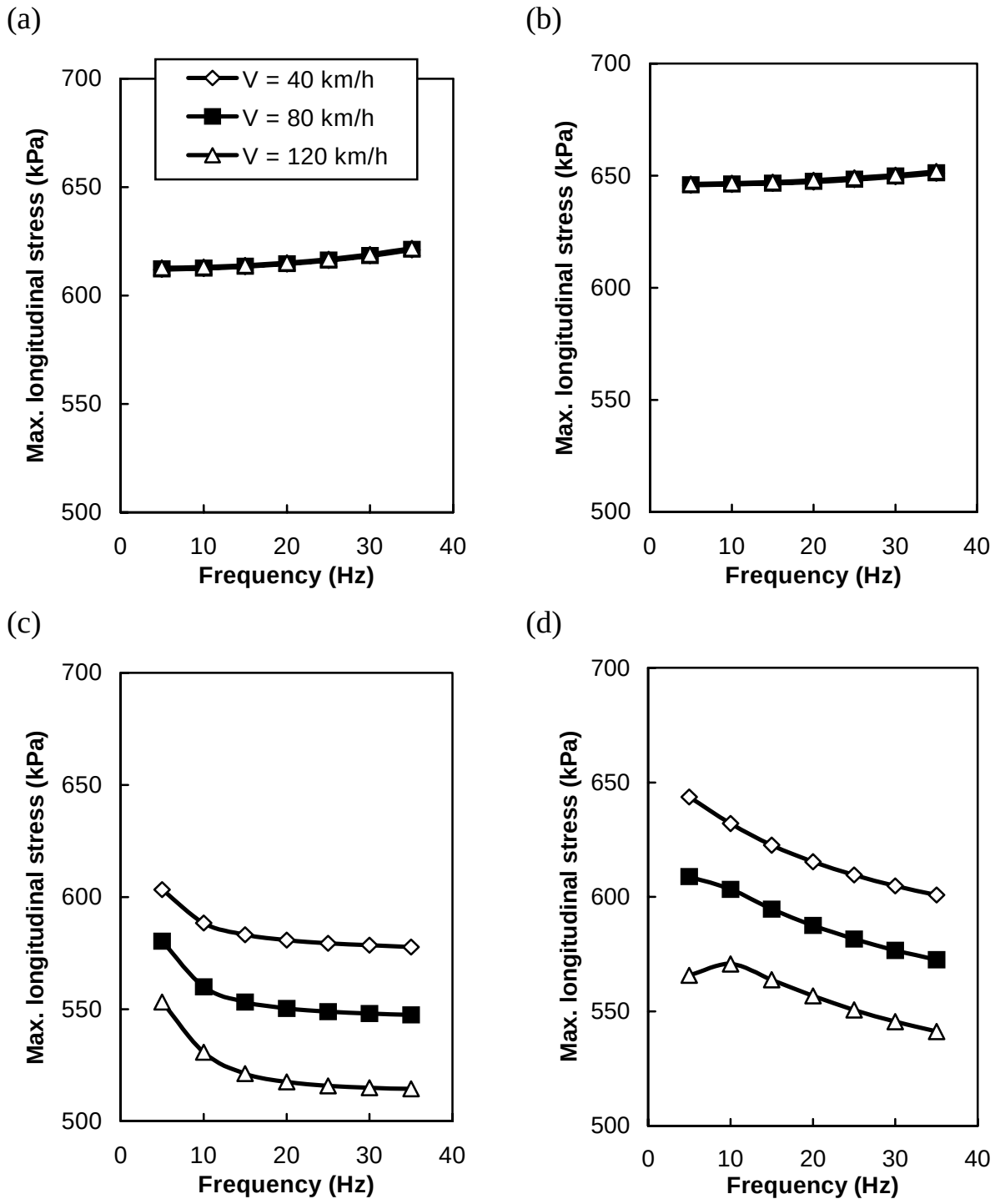

Figure 3.8. Effect of load frequency on maximum longitudinal stress: (a) phase = 0, c = 0; (b) phase = 180 deg., c = 0; (c) phase = 0, c = 12 MPa sec/m; (d) phase = 180 deg., c = 12 MPa sec/m (1 kPa = 0.145 psi, 1 km/h = 0.63 mph, 1 MPa sec/m = 3.69 psi sec/in.)

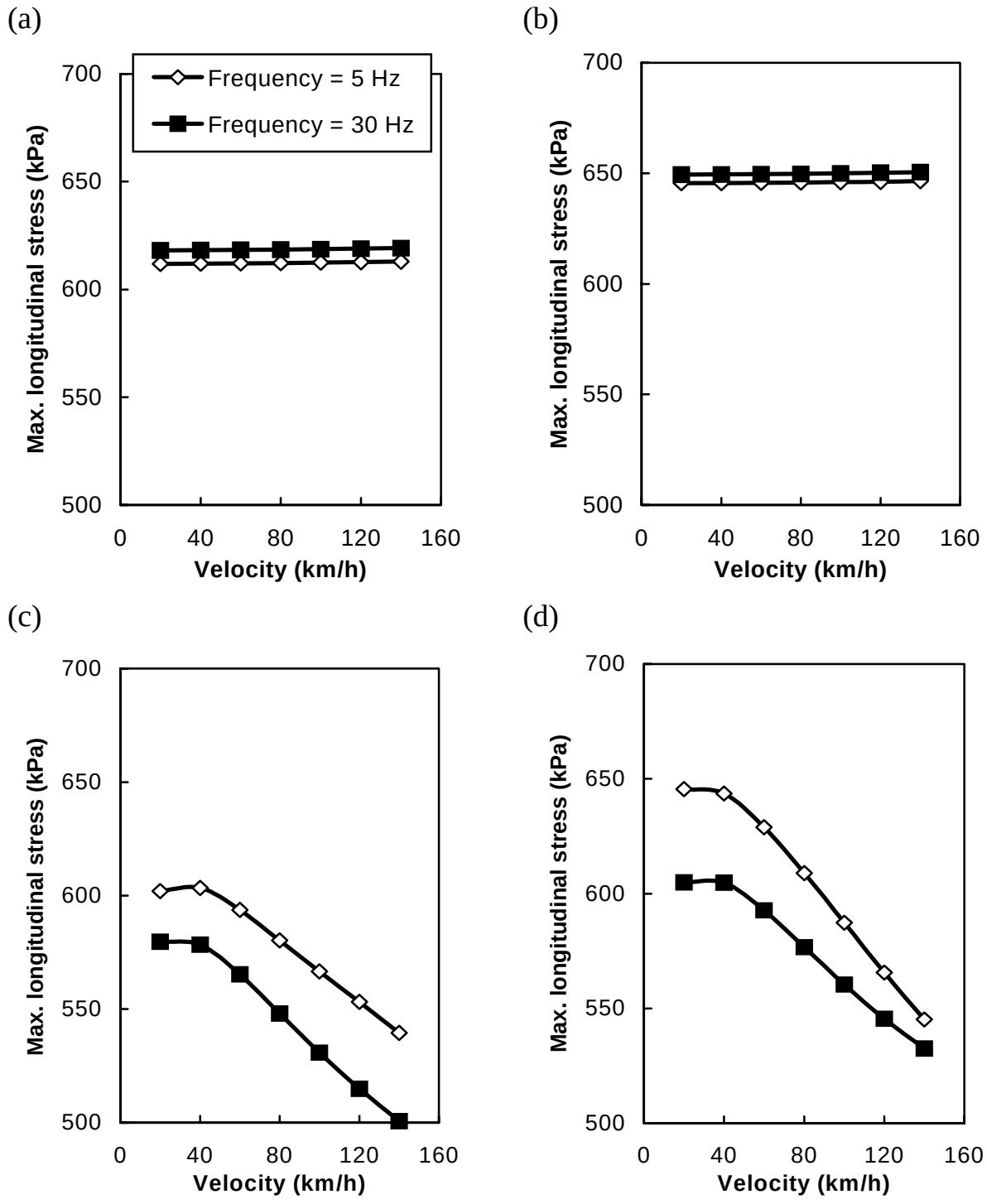

Figure 3.9. Effect of velocity on maximum longitudinal stress: (a) phase = 0, c = 0; (b) phase = 180 deg., c = 0; (c) phase = 0, c = 12 MPa sec/m; (d) phase = 180 deg., c = 12 MPa sec/m (1 kPa = 0.145 psi, 1 km/h = 0.63 mph, 1 MPa sec/m = 3.69 psi sec/in.)

(a)

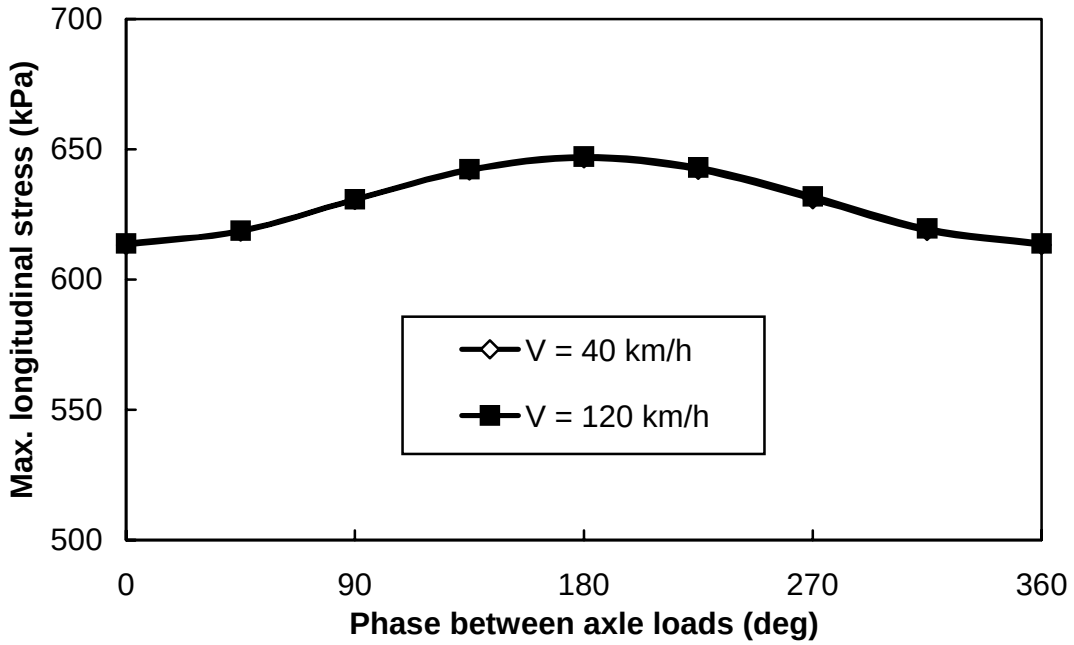

(b)

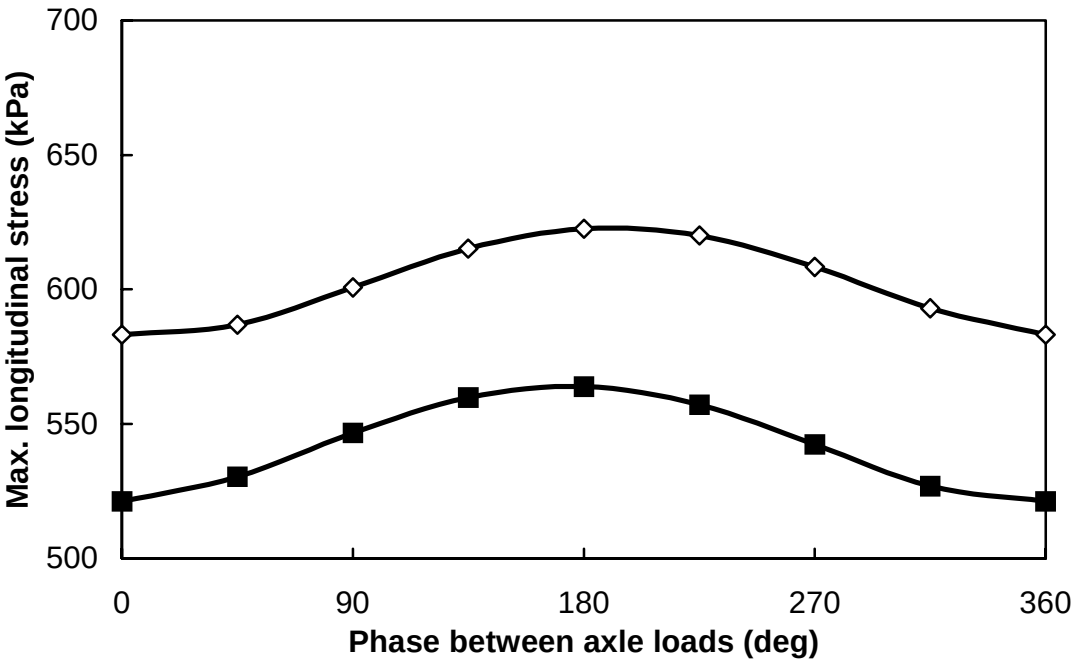

Figure 3.10. Effect of phase between front- and rear-axle loads on maximum longitudinal stress when load frequency = 15 Hz: (a) c = 0; (b) c = 12 MPa sec/m (1 kPa = 0.145 psi, 1 MPa sec/m = 3.69 psi sec/in.)

(a)

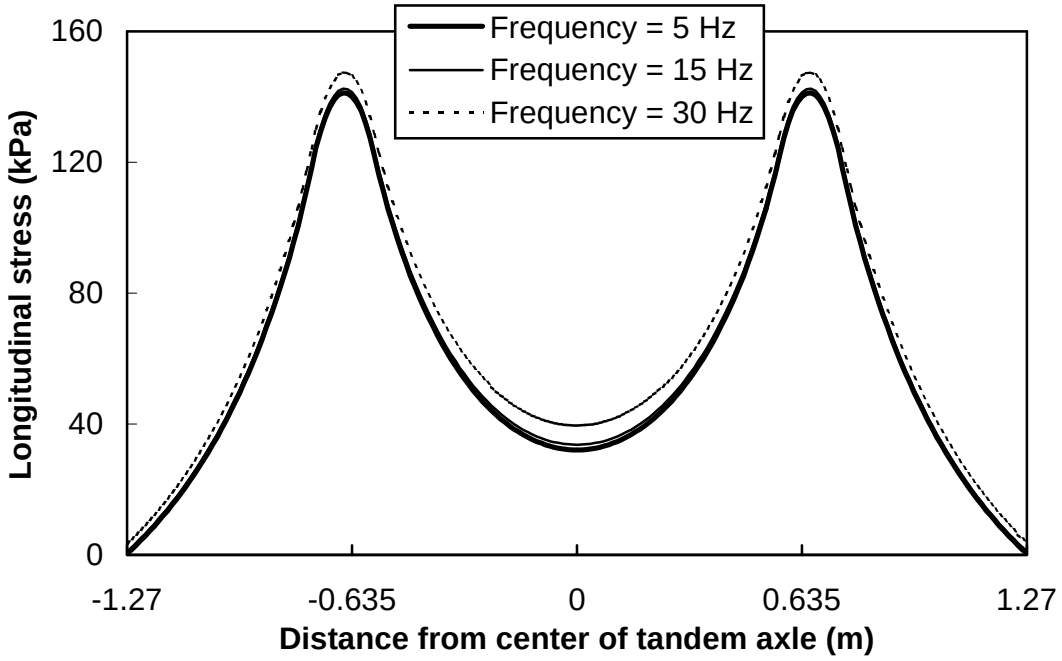

(b)

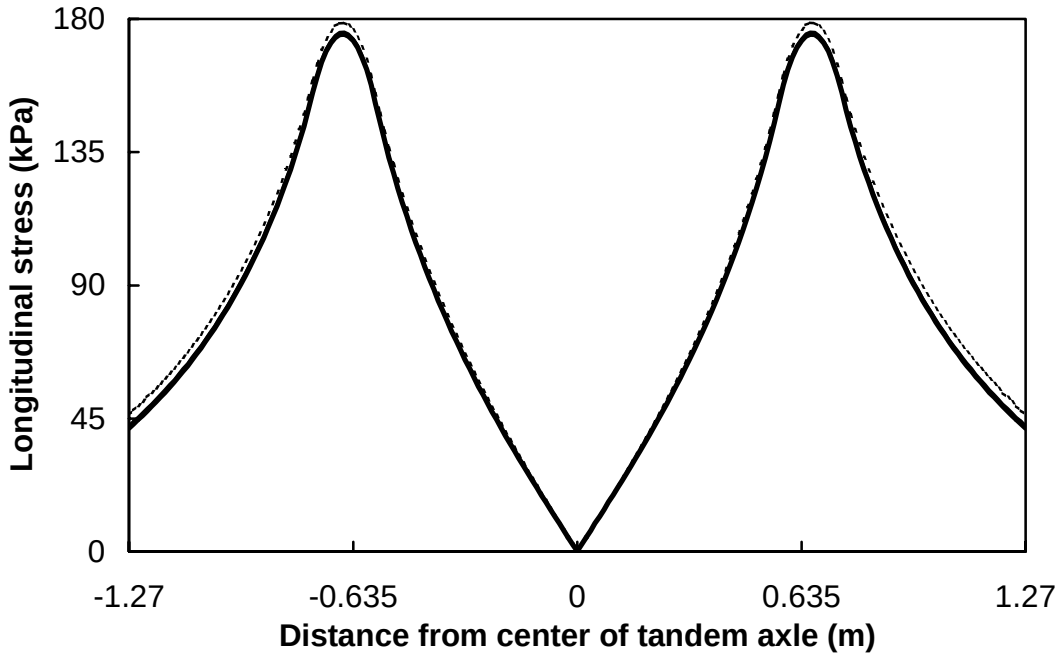

Figure 3.11. Maximum stress distribution for various load frequencies when V = 40 km/h and c = 0: (a) phase = 0; (b) phase = 180 deg. (1 kPa = 0.145 psi, 1 m = 3.28 ft)

(a)

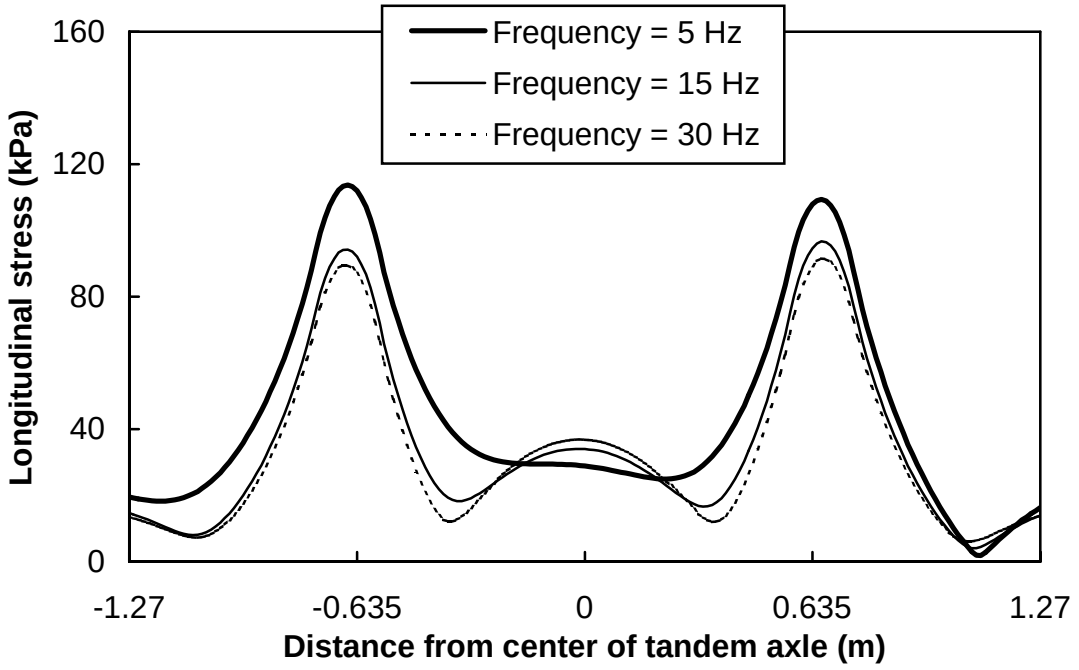

(b)

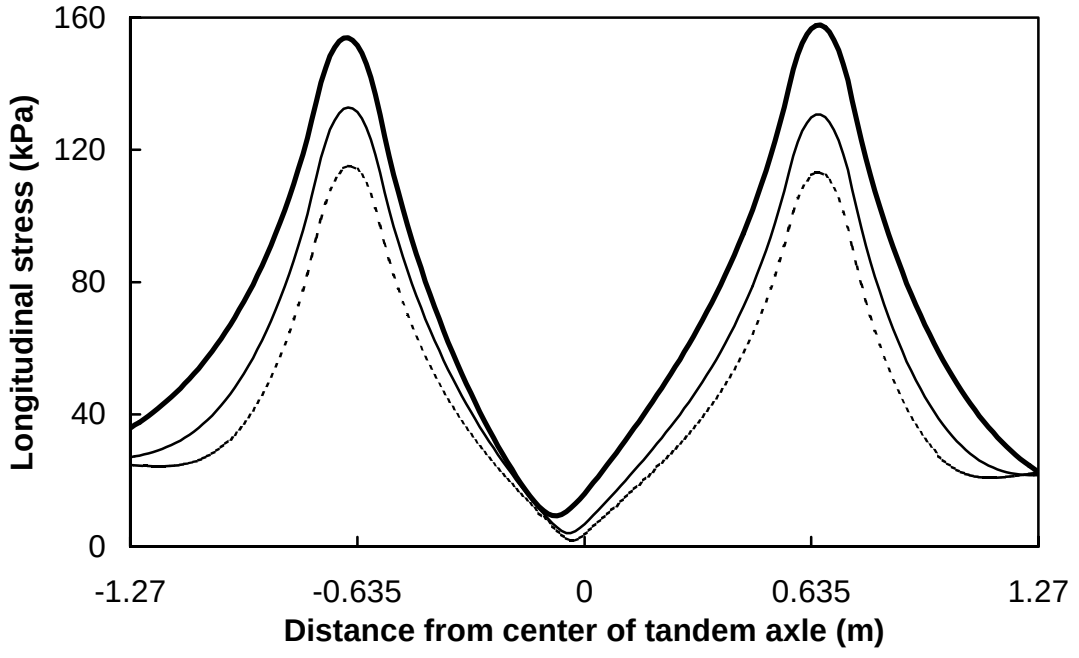

Figure 3.12. Maximum stress distribution for various load frequencies when V = 40 km/h and c = 12 MPa sec/m: (a) phase = 0; (b) phase = 180 deg. (1 kPa = 0.145 psi, 1 m = 3.28 ft)

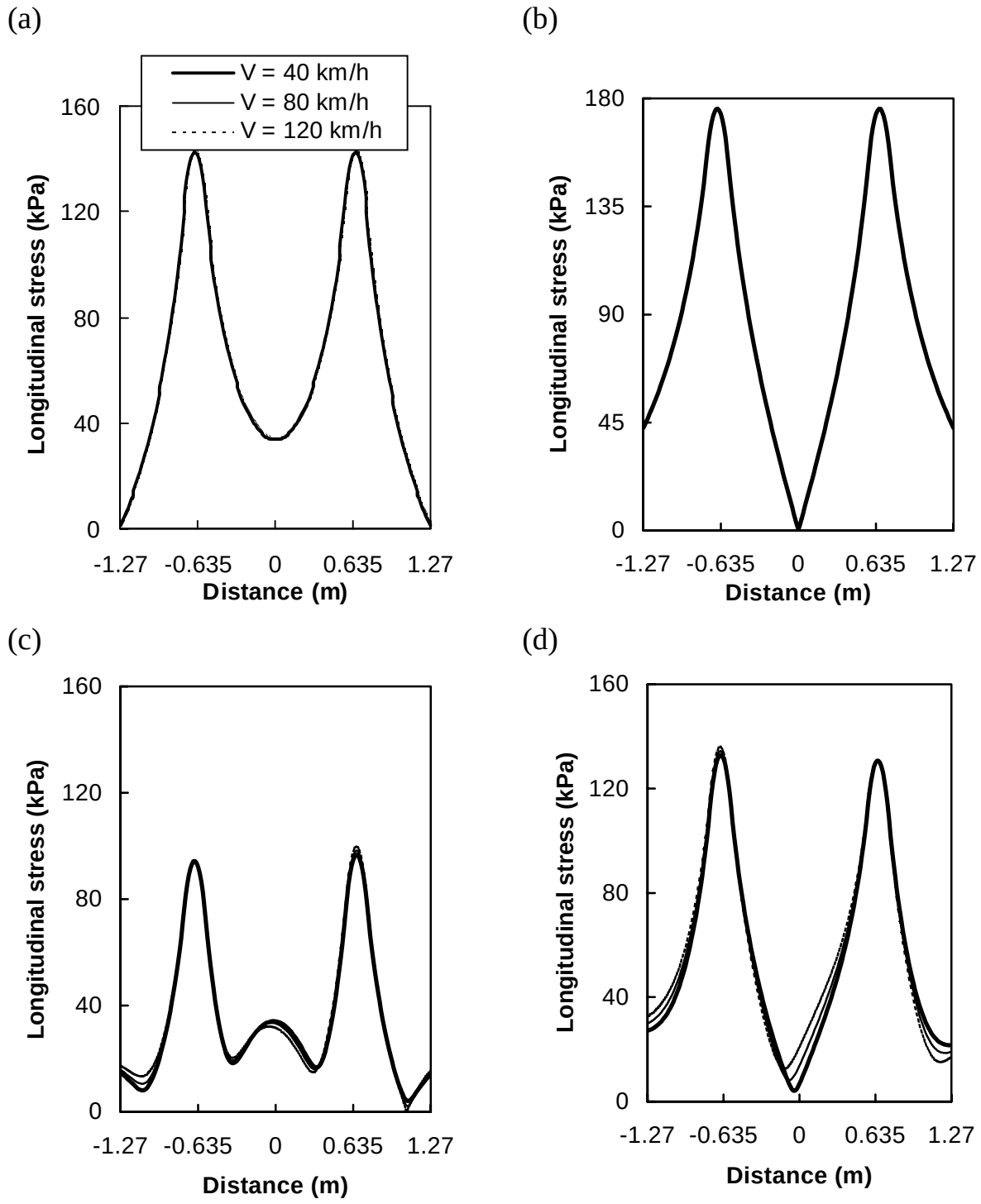

Figure 3.13. Maximum stress distribution for various velocities when frequency = 15 Hz: (a) c = 0, phase = 0; (b) c = 0, phase = 180 deg.; (c) c = 12 MPa sec/m, phase = 0; (d) c = 12 MPa sec/m, phase = 180 deg. (1 kPa = 0.145 psi, 1 m = 3.28 ft, 1 km/h = 0.63 mph)

(a)

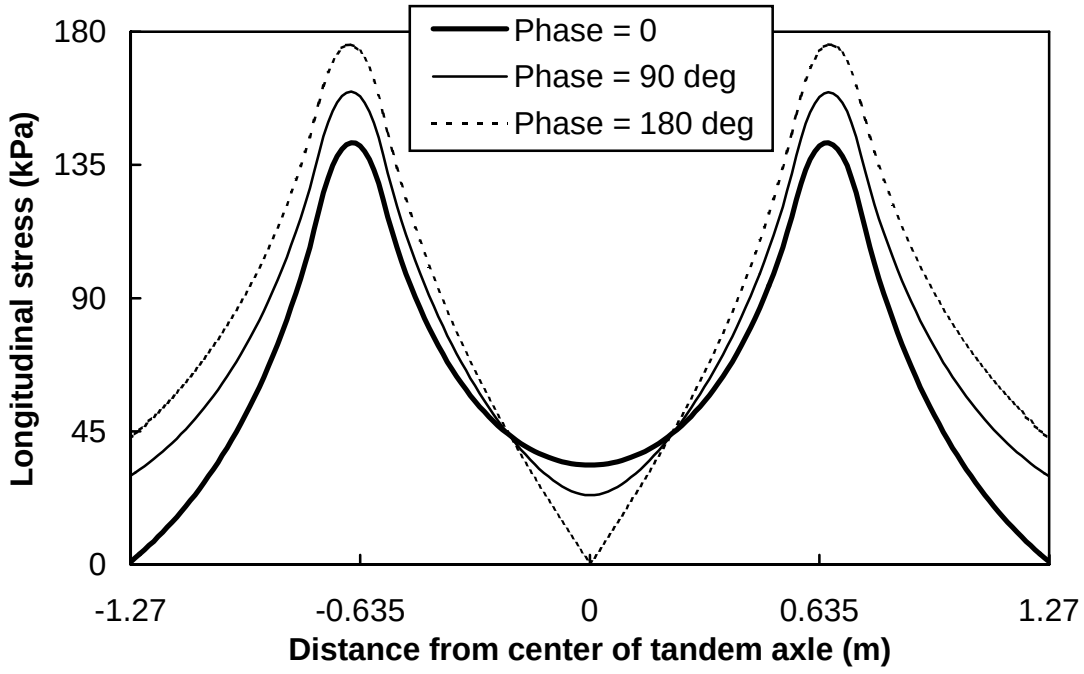

(b)

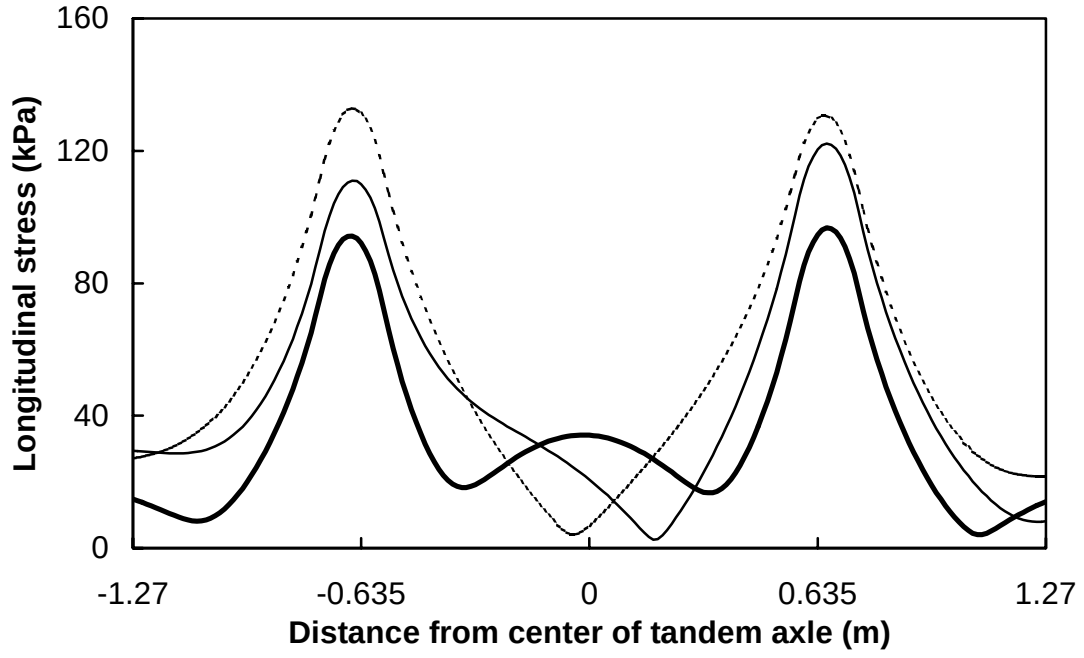

Figure 3.14. Maximum longitudinal stress distribution for various phases when V = 40 km/h and frequency = 15 Hz: (a) c = 0; (b) c = 12 MPa sec/m (1 kPa = 0.145 psi, 1 m = 3.28 ft)

3.4 SUMMARY

This project has investigated the dynamic stress response of concrete pavements under moving tandem-axle loads of constant amplitude and harmonic and arbitrary variations. The concrete pavement has been modeled using a plate of infinite extent on a viscoelastic foundation. As explained in the previous chapter, we have developed formulations in the transformed field domains of time, space, and moving space. The analysis results show the following:

- For the moving tandem-axle loads of constant amplitude,
  - Without viscous damping, the stress distribution is symmetric with respect to the midpoint of the tandem-axle loads, and the maximum stress remains almost the same regardless of velocity.
  - With viscous damping, the stress distribution is no longer symmetric, and the maximum stress initially increases slightly and then decreases with increasing velocity. The peak stress under the front-axle loads decreases as viscous damping increases, and the maximum stress occurs under the rear-axle loads.
- For the moving tandem-axle loads of arbitrary variation caused by pavement surface roughness, the maximum load amplitude and stress increase significantly compared with those obtained with the perfectly smooth pavement.
- For the moving tandem-axle loads of harmonic variation;
  - Without viscous damping, the maximum stress is not much affected by the load frequency.
  - With viscous damping, the stress distribution is affected significantly by the load frequency, and the maximum stress decreases as the load frequency increases.
  - Regardless of viscous damping, the velocity does not much affect the stresses, and the peak stresses under the front- and rear-axle loads are similar to each other. As the phase between the front- and rear-axle loads increases, the maximum stress becomes significantly larger.

CHAPTER 4. FLEXIBLE PAVEMENT RESPONSE TO MOVING DYNAMIC TANDEM-AXLE LOADS

4.1 RESPONSE TO MOVING LOADS OF CONSTANT AMPLITUDE

We first investigated the displacement and stress responses of the flexible pavements at the bottom of the surface layer that result from moving loads with a constant amplitude. The material properties and geometry of the flexible pavement model and the dimensions of the tandem-axle loads used in this study (Figure 2.1) are listed in Table 4.1. For the FFT in the moving and fixed spaces and transformed field domains of those spaces, we used 2,048 for the number of transformed points and 1.27 cm (0.5 in.) for the distance increment. The stresses considered in this study are tensile stresses in the longitudinal direction at the bottom of surface layer because transverse stresses are smaller than longitudinal stresses.

Table 4.1. Material properties and load geometry for flexible pavement model

E	3,445 MPa (500 ksi)	d_1	17.78 cm (7 in.)
ν	0.35	d_2	20.32 cm (8 in.)
k	27.2 MN/m^3 (100 pci)	d_t	33 cm (13 in.)
h	15.24 cm (6 in.)	d_w	188 cm (74 in.)
m	354 kg/m^2 (0.001305 lb sec^2/in^3)	d_a	132 cm (52 in.)
D	0.2 %	c	6 MPa sec/m (22.12 lb sec/in^3)
Axle load	-80 kN (-18 kip)		

The differences in the responses under dual-wheel, dual-wheel single-axle, and dual-wheel tandem-axle loads have been investigated first with a velocity of 40 km/h (25 mph), as shown in Figure 4.1. If the flexible pavement is sufficiently large and the velocity is constant, the response to the moving loads will remain constant at any instant along the moving axis. This means that the displacement and stress distributions are moving with the loads. The displacement and stress distributions along the moving axis in the figure are shown at the y coordinate where the maximum deflection or stress occurs. The location of the maximum response varies depending on the material properties, velocity, and load configurations. The 0 distance in the figure represents the midpoint between the two axles. Dual-wheel and dual-wheel single-axle loads yield almost the same responses except that the dual-wheel single-axle loads yield a slightly larger maximum stress with no viscous damping. For the displacements, shown in Figure 4.1(*a*), the tandem-axle loads cause larger maximum

deflections than those obtained with the other loads, and the differences become significant with viscous damping. Without viscous damping, the shape of pavement deflections is almost symmetric; however, with viscous damping, the shape is no longer symmetric, the peak displacement near the front-axle loads decreases, and the maximum deflection occurs near the rear-axle loads. Note that because the material damping (linear hysteretic damping) of the system in this study is very small (D = 0.2 %), the response is essentially symmetric when there is no viscous damping. However, if material damping is large, the response is not symmetric (Refs 7, 13). For the stresses (Figure 4.1(*b*)), the tandem-axle loads yield slightly smaller maximum stress when there is no damping; however, with viscous damping, the maximum stresses near the loads are almost identical for the three loading cases. For the rest of this paper, the responses from only tandem-axle, not single-axle, applications are presented because the tandem-axle loads cause most deflections and stresses comparable to single-axle loads and resulting pavement distresses.

We next investigated the effects of velocity and material properties on the maximum deflection and stress. Figures 4.2(*a*) and (*b*) show the effect of velocity for various viscous damping values. The logical values of the velocities up to 150 km/h (95 mph) are used in this study. If the system has no viscous damping, the increase in the maximum deflection and stress with velocity is negligible. If there is viscous damping, the maximum deflection and stress decrease as the velocity becomes larger. As the viscous damping constant increases, shown in Figures 4.2(*c*) and (*d*), the maximum deflection and stress decrease significantly. It should be noted that the viscous damping constant depends largely on the binder contents in the asphalt mixtures and the types and moisture contents of underlying layers such as base, sub-base, and subgrade. Figure 4.3 shows the effects of the stiffness of foundation and elastic modulus of surface layer on the maximum deflection and stress with viscous damping. The maximum deflection and stress decrease as the stiffness of foundation increases, as shown in Figures 4.3(*a*) and (*b*), with more pronounced effect on deflections than on stresses. As shown in Figure 4.3(*c*), the maximum deflection decreases as the elastic modulus of the surface layer becomes larger; on the other hand, the maximum stress increases significantly as the elastic modulus increases, as shown in Figure 4.3(*d*).

4.2 RESPONSE TO MOVING ARBITRARY LOADS

The roughness of the pavement surface will cause a variation in load amplitude when a truck is moving. We have investigated the displacement and stress responses that result from this arbitrary variation of the load. Eqs. 2.5, 2.6, 2.7, and 2.27 are used to calculate stresses. As explained in the previous chapter, to obtain the time histories of the dynamic forces on the front and rear tandem-axle tires, a computer program developed to predict the wheel loads in the TxMLS research project has been used with three different pavement profiles (Refs 15, 16). One is a perfectly smooth profile and the others are profiles corresponding to PSI values of 4.5 and 2.0. Figure 3.4 shows the dynamic loads caused by various pavement roughnesses under the wheels of the front and rear tandem axles when a velocity is 32 km/h (20 mph).

(a)

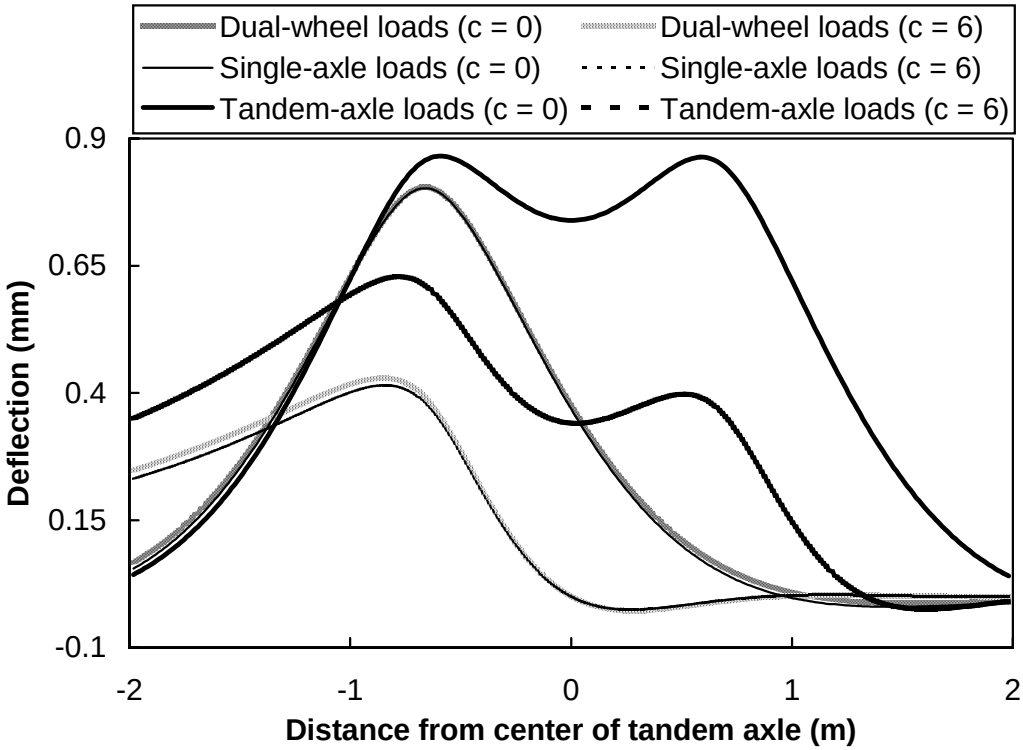

(b)

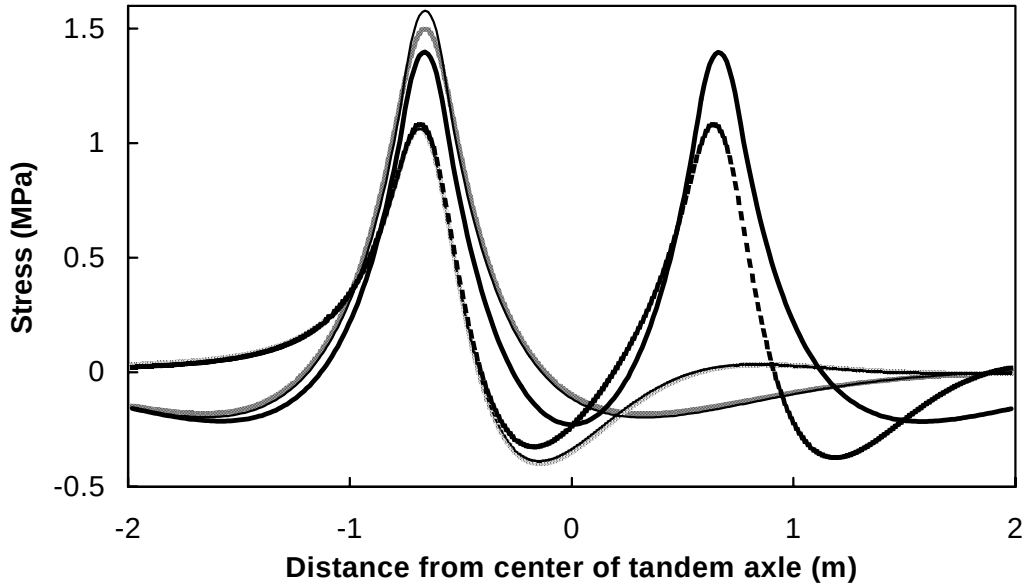

Figure 4.1. Comparison of responses among dual-wheel, single-axle, and tandem-axle loads: (a) on displacements; (b) on stresses (unit of c = MPa sec/m) (1 MPa = 145 psi, 1 m = 3.28 ft, 1 mm = 0.0394 in., 1 MPa sec/m = 3.69 psi sec/in.)

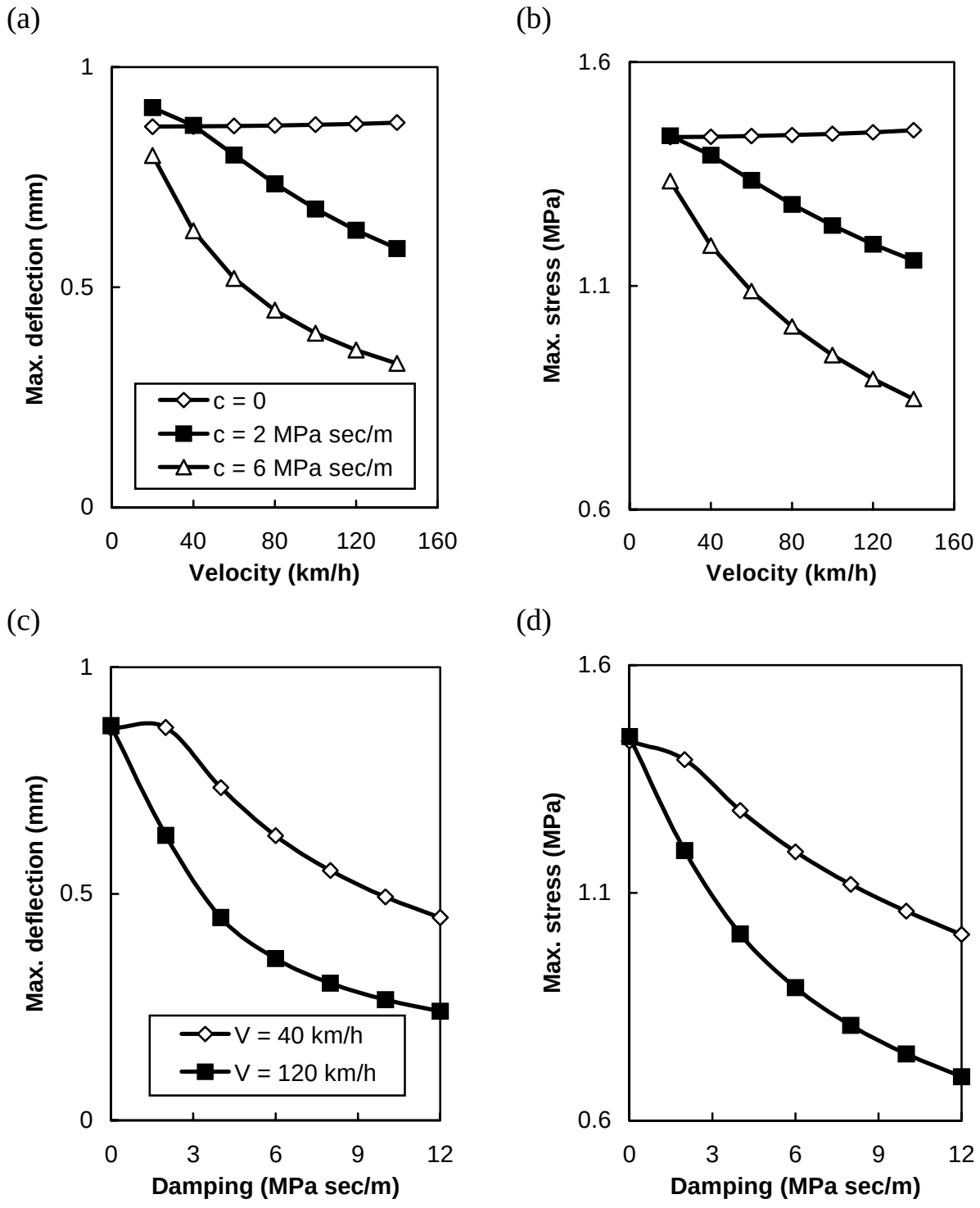

Figure 4.2. Effects of velocity and viscous damping on maximum deflection and stress (1 MPa = 145 psi, 1 mm = 0.0394 in., 1 MPa sec/m = 3.69 psi sec/in., 1 km/h = 0.63 mph)

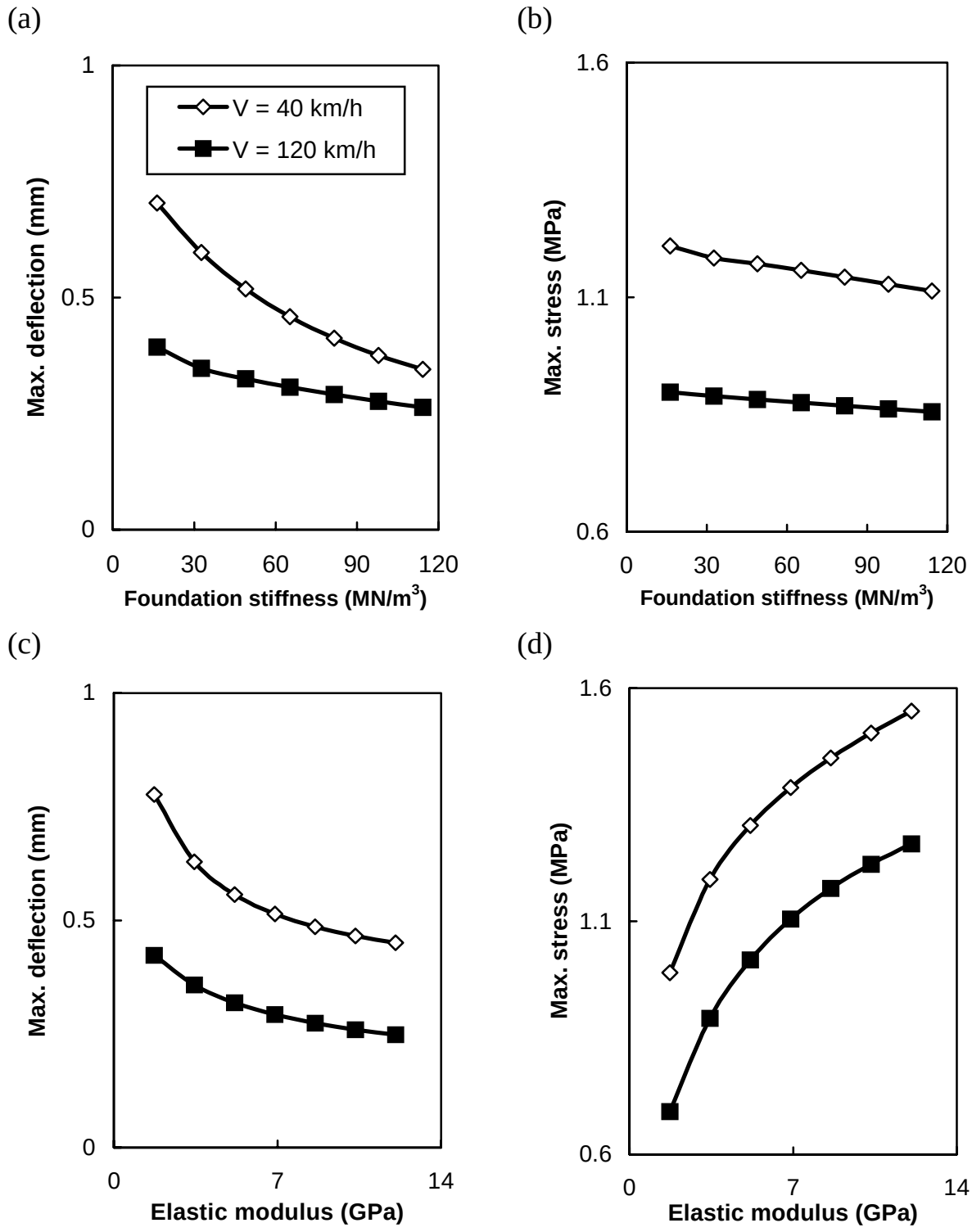

Figure 4.3. Effects of foundation stiffness and elastic modulus on maximum deflection and stress (1 MPa = 145 psi, 1 mm = 0.0394 in., 1 MN/m^3 = 3.68 pci, 1 km/h = 0.63 mph)

The time histories of deflections and stresses under the front- and rear-axle tires at the coordinates of $\{\eta_0 + 132 \text{ cm}, y_0 + 4 \text{ cm}\}$ and $\{\eta_0, y_0 + 4 \text{ cm}\}$ are shown in Figures 4.4 and 4.5, respectively. The time histories of the deflection and stress are similar to those of the load (Figure 3.4). The deflections under the rear-axle tires are larger than those under the front-axle tires, as shown in Figure 4.4. The increments of the maximum deflections on the PSI 2.0 pavement, compared with the ideal pavement are about 28 percent and 25 percent under the front- and rear-axle tires, respectively. The stresses under the front- and rear-axle tires are similar (Figure 4.5), and the maximum stresses on the PSI 2.0 pavement are about 30 percent greater than the stress on the perfectly smooth pavement. This analysis shows a significant effect of pavement roughness on wheel-load deflections and stresses as well as on the subsequent rutting and fatigue life of pavements. This analysis supports the specification changes state highway agencies have been making to improve pavement smoothness.

4.3 RESPONSE TO MOVING HARMONIC LOADS

As discussed above, the actual loads cause variations in amplitude because of the surface roughness, and there is a phase between the front- and rear-axle loads. It was also shown that these variations affect pavement responses significantly. In order to further investigate the effect of the load variation on the responses, we considered the moving tandem-axle loads with harmonic variations. Figures 4.6 and 4.7 show the displacement and stress distributions near the loads along the moving axis with a velocity of 40 km/h (25 mph). Because the responses under the moving harmonic loads change with time, the figures show the maximum amplitudes of the responses along the moving coordinates, and those shapes do not necessarily occur at the same time. When there is no viscous damping, as shown in Figure 4.6(*a*), the displacement distributions are symmetric with respect to the midpoint between the two axles and the maximum deflection increases as the load frequency increases. Also, for a given frequency, a phase of 0 degrees causes higher deflections than a phase of 180 degrees. The 0 deflection with a phase of 180 degrees at the midpoint between the two axles is obtained because the influence of the front- and rear-axle loads is the same and the signs of the deflections resulting from those loads are opposite. If there is viscous damping (Figure 4.6(*b*)), the distribution is no longer symmetric and the maximum deflections are smaller than those without viscous damping. Note also that the maximum deflections decrease as frequency increases, which is an effect opposite to that of no viscous damping. Compared with the results without viscous damping, the effect of frequency on deflections is more pronounced. In addition, the effect of phase is more pronounced at a low frequency than at a high one. For the stress distributions without damping, shown in Figure 4.7(*a*), frequency does not have a significant effect, but phase does. In distributions with viscous damping, shown in Figure 4.7(*b*), frequency has a substantial effect on stresses. On the other hand, phase has only a moderate effect.

(a)

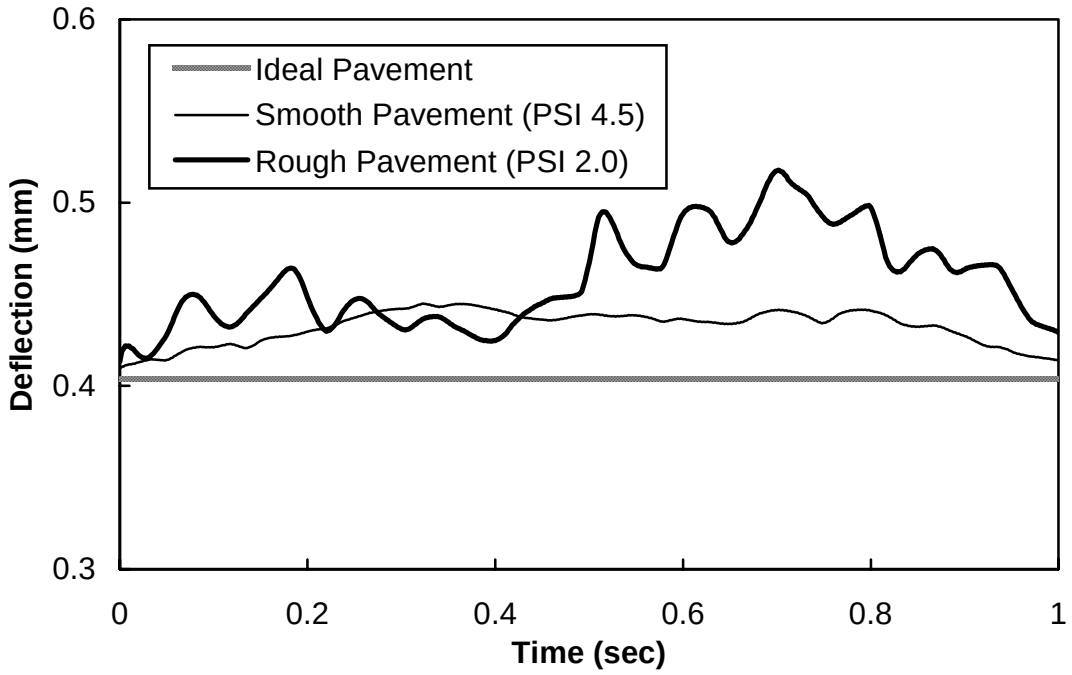

(b)

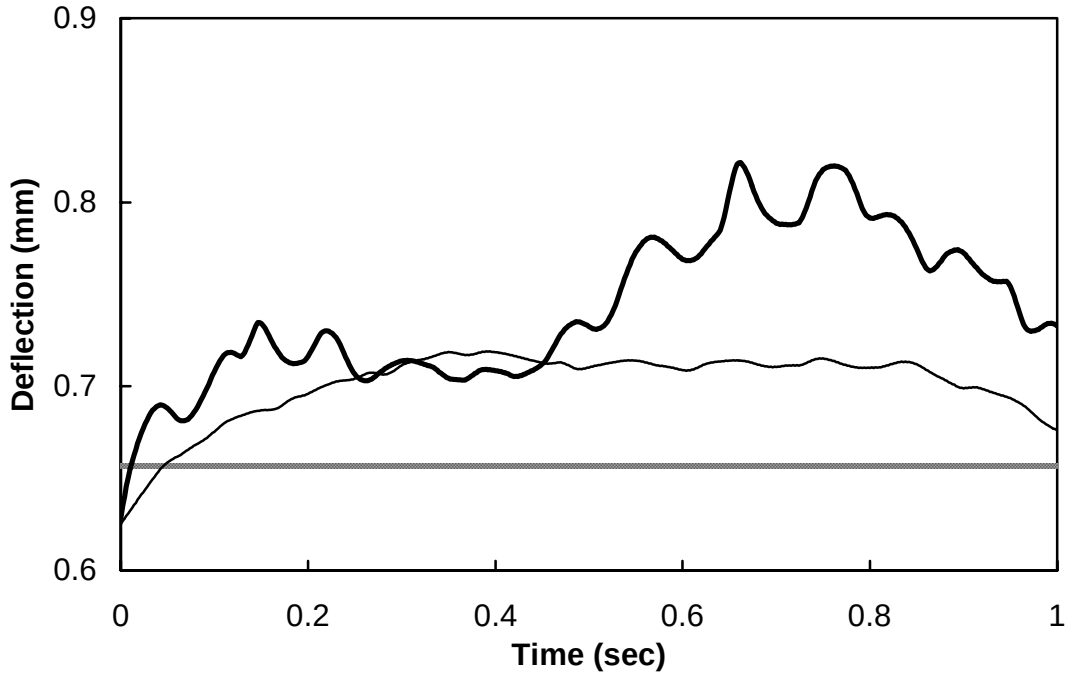

Figure 4.4. Time history of deflection for various pavement surface roughnesses: (a) under front-axle tires; (b) under rear-axle tires (1 mm = 0.0394 in.)

(a)

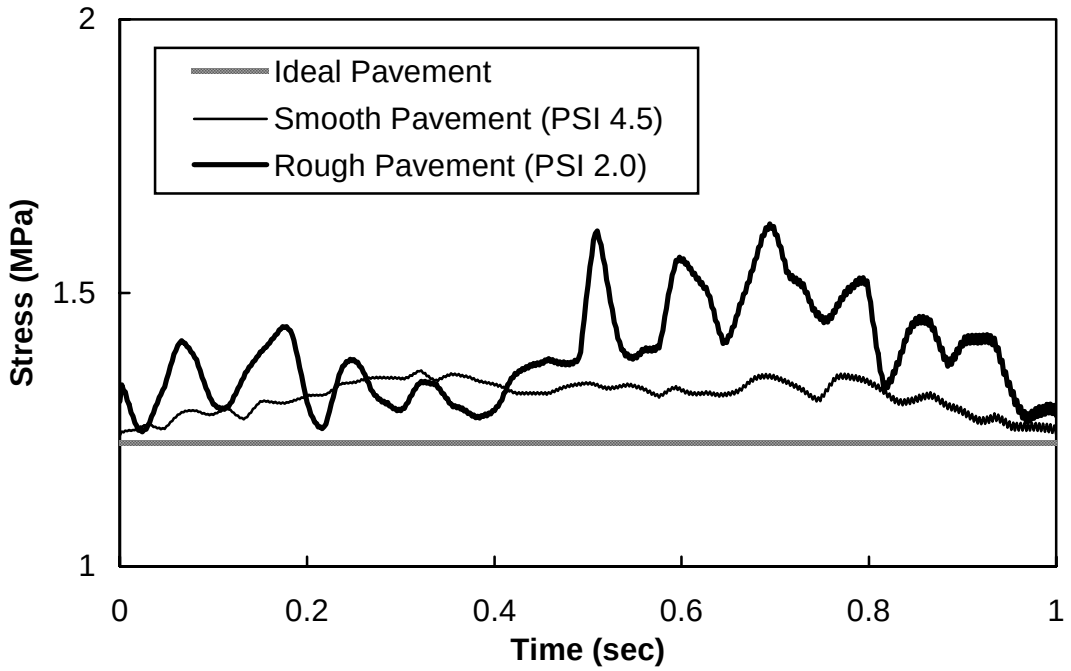

(b)

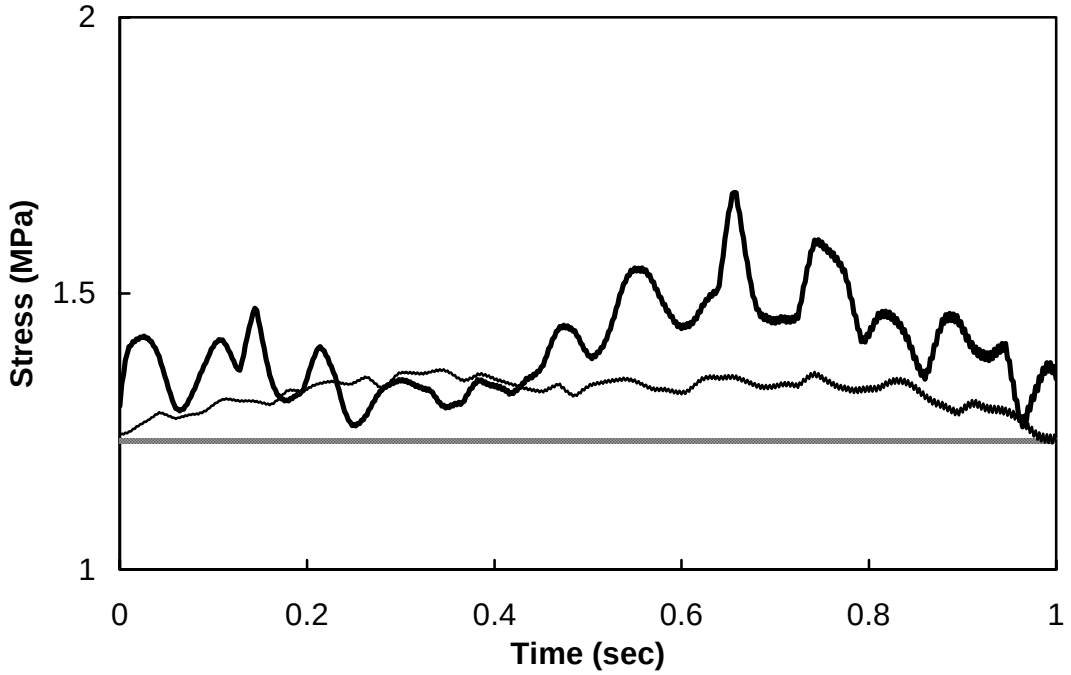

Figure 4.5. Time history of stress for various pavement surface roughnesses: (a) under front-axle tires; (b) under rear-axle tires (1 MPa = 145 psi)

(a)

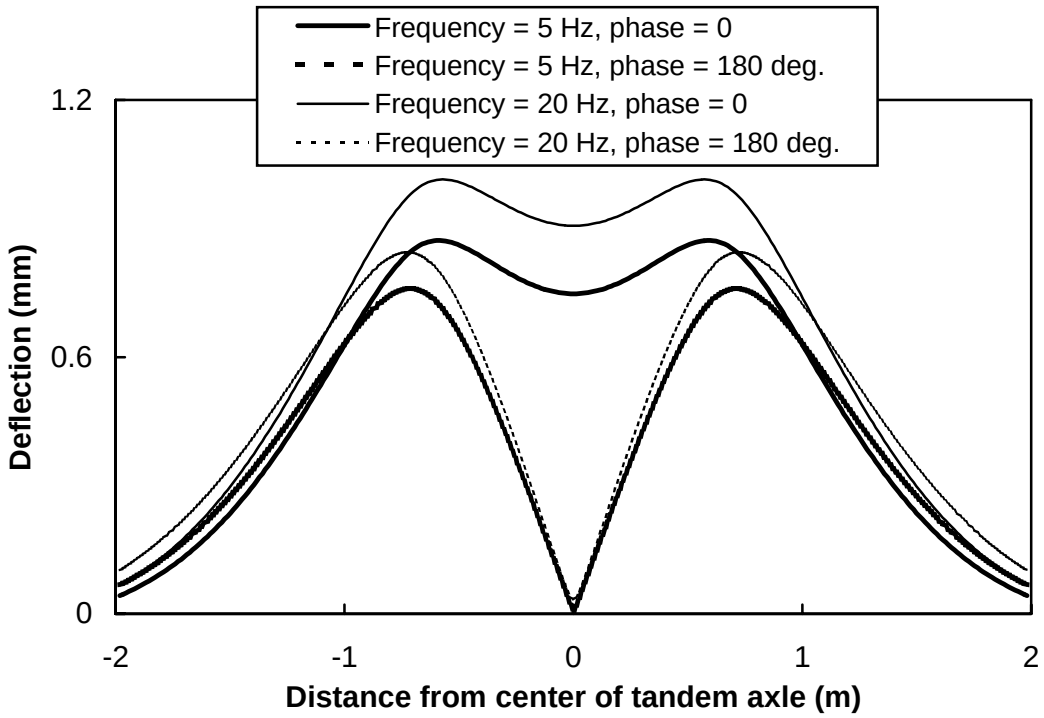

(b)

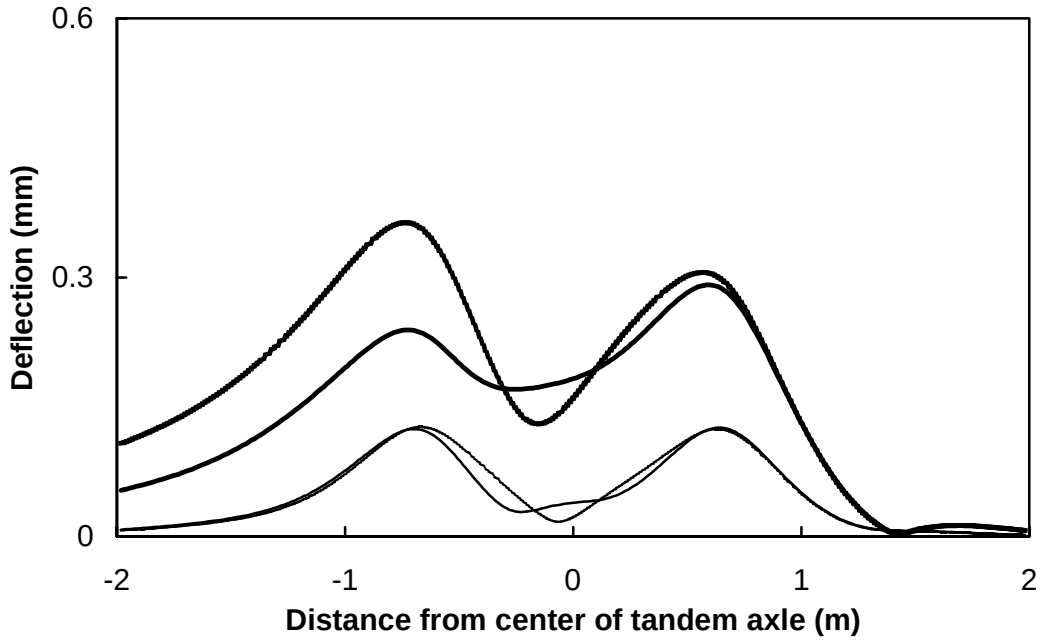

Figure 4.6. Displacement distribution: (a) when c = 0; (b) when c = 6 MPa sec/m (1 mm = 0.0394 in., 1 m = 3.28 ft)

(a)

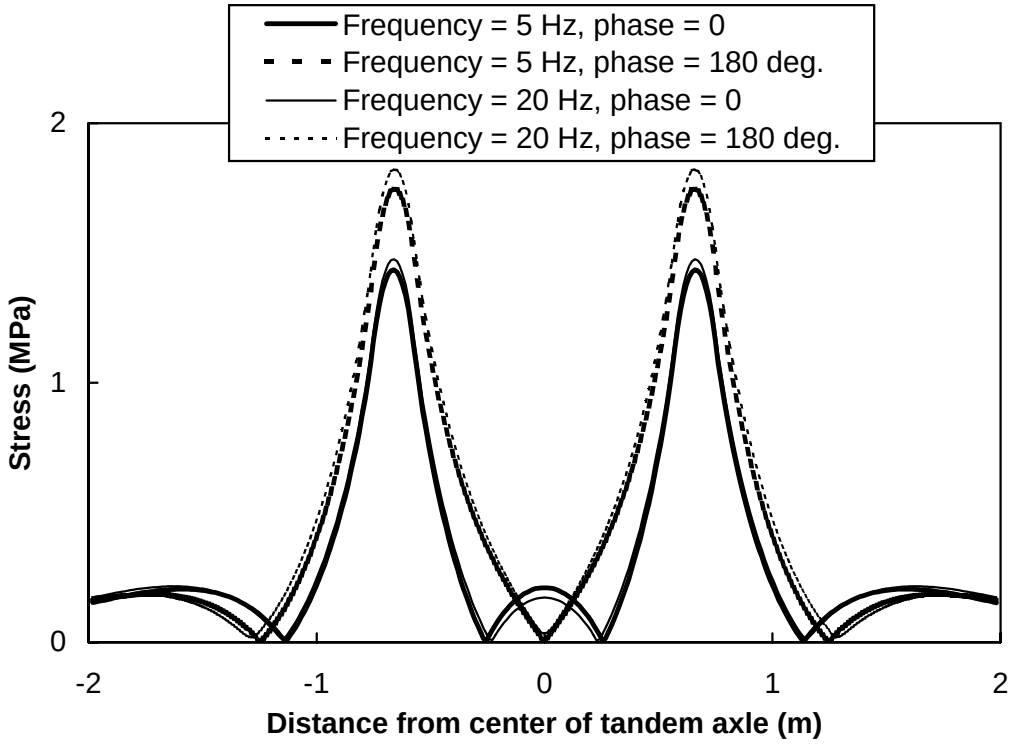

(b)

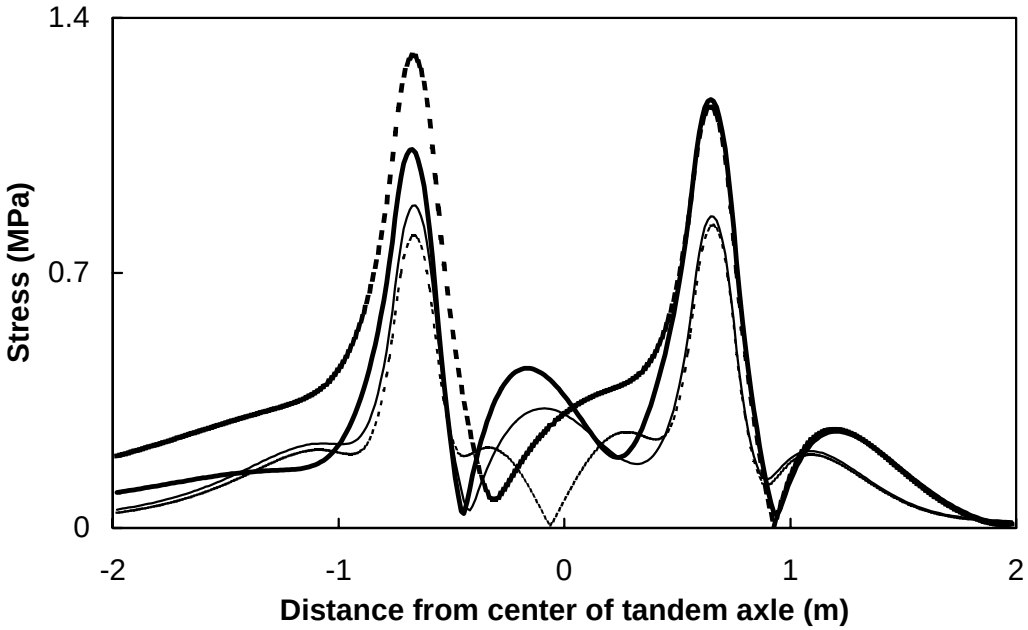

Figure 4.7. Stress distribution: (a) when c = 0; (b) when c = 6 MPa sec/m (1 MPa = 145 psi, 1 m = 3.28 ft)

Further studies have been conducted to investigate the effects of frequency, velocity, and phase on the maximum deflection and stress with viscous damping. Figure 4.8 shows the effect of load frequency. For a low velocity of 40 km/h (25 mph), the maximum deflections and stresses decrease as the frequency increases. With a high velocity of 120 km/h (76 mph), the maximum deflections decrease as the frequency increases if there is no phase (Figure 4.8(*a*)); however, with a phase of 180 degrees (Figure 4.8(*b*)), the maximum deflections increase initially and then decrease as the frequency becomes larger. This relationship can also be observed for the maximum stresses, as shown in Figures 4.8(*c*) and (*d*). The effect of velocity on deflections and stresses is shown in Figure 4.9. With a phase of zero degrees, frequency has a significant effect on deflections, while its effect on stresses is more pronounced at low velocities than at high ones (Figures 4.9(*a*) and (*c*)). For a phase angle of 180 degrees, velocity has a substantial effect on the deflections at a frequency of 5 Hz, with deflections decreasing as velocity increases over 50 km/h. At a frequency of 20 Hz, deflections increase with the velocity. As for the effect on stresses, velocity does not have a significant effect at a frequency of 20 Hz, but at 5 Hz frequency, stresses decrease with velocity for both phases. The effect of phase between the front- and rear-axle loads is shown in Figure 4.10. At the frequency of 5 Hz, the phase effect is more pronounced on deflections than on stresses. At the frequency of 20 Hz, the phase angle has a more pronounced effect on deflections and stresses at a high velocity than at a low velocity. This phase effect cannot be obtained with single-axle loads; therefore, the use of tandem-axle loads to find the accurate pavement response is necessary.

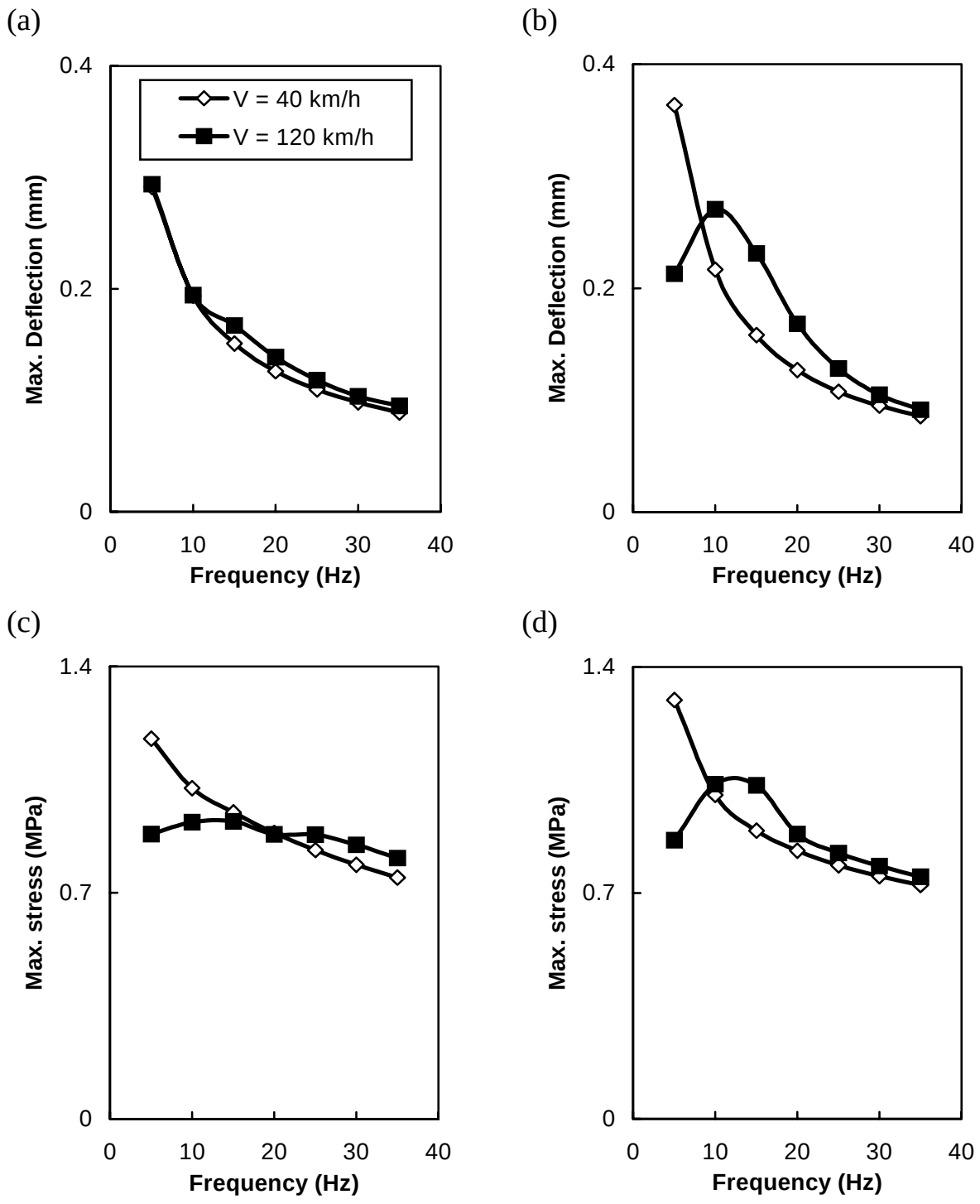

Figure 4.8. Effect of load frequency: (a) on maximum deflection when phase = 0; (b) when phase = 180 deg.; (c) on maximum stress when phase = 0; (d) when phase = 180 deg. (1 MPa = 145 psi, 1 mm = 0.0394 in., 1 km/h = 0.63 mph)

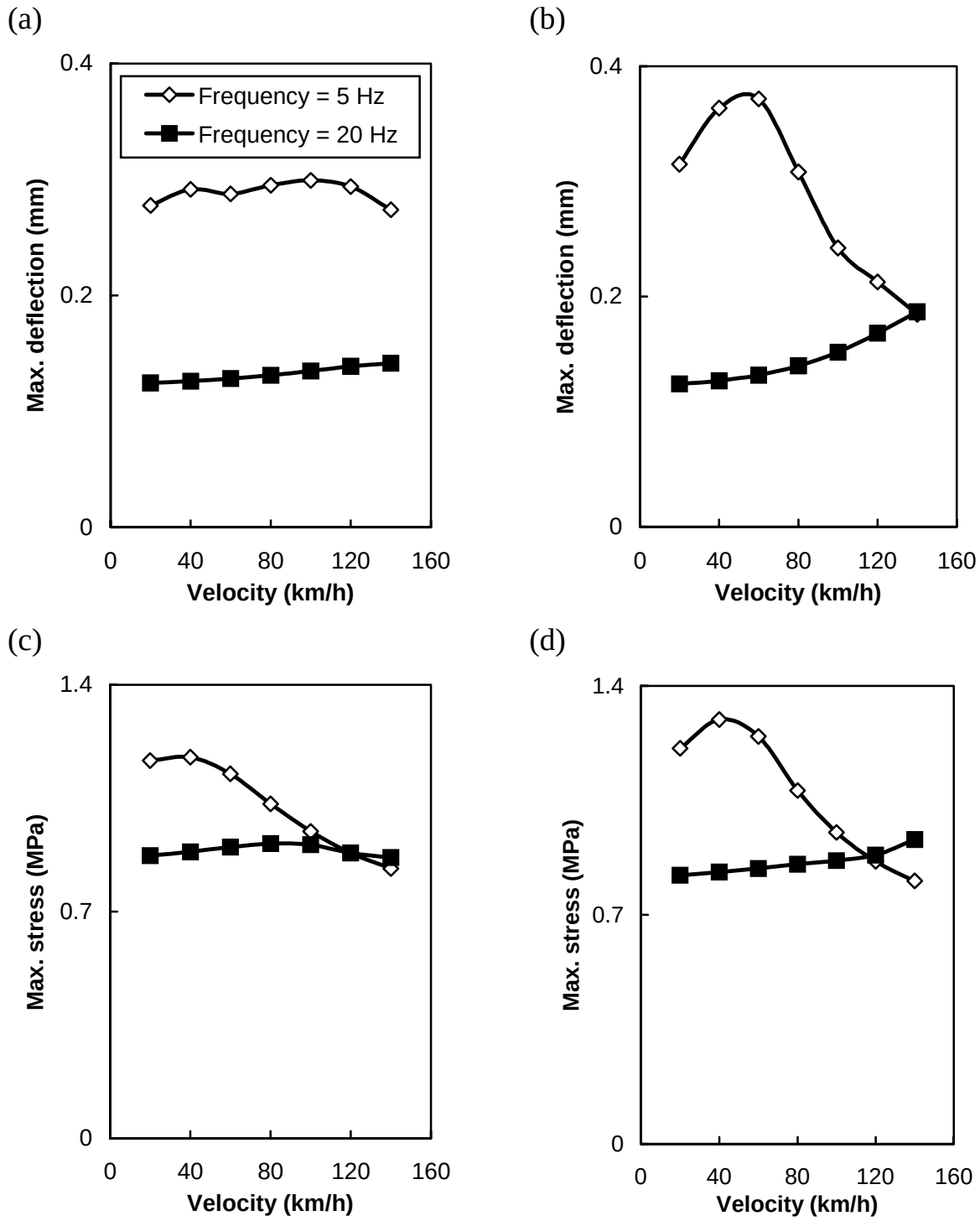

Figure 4.9. Effect of velocity: (a) on maximum deflection when phase = 0; (b) when phase = 180 deg.; (c) on maximum stress when phase = 0; (d) when phase = 180 deg. (1 MPa = 145 psi, 1 mm = 0.0394 in., 1 km/h = 0.63 mph)

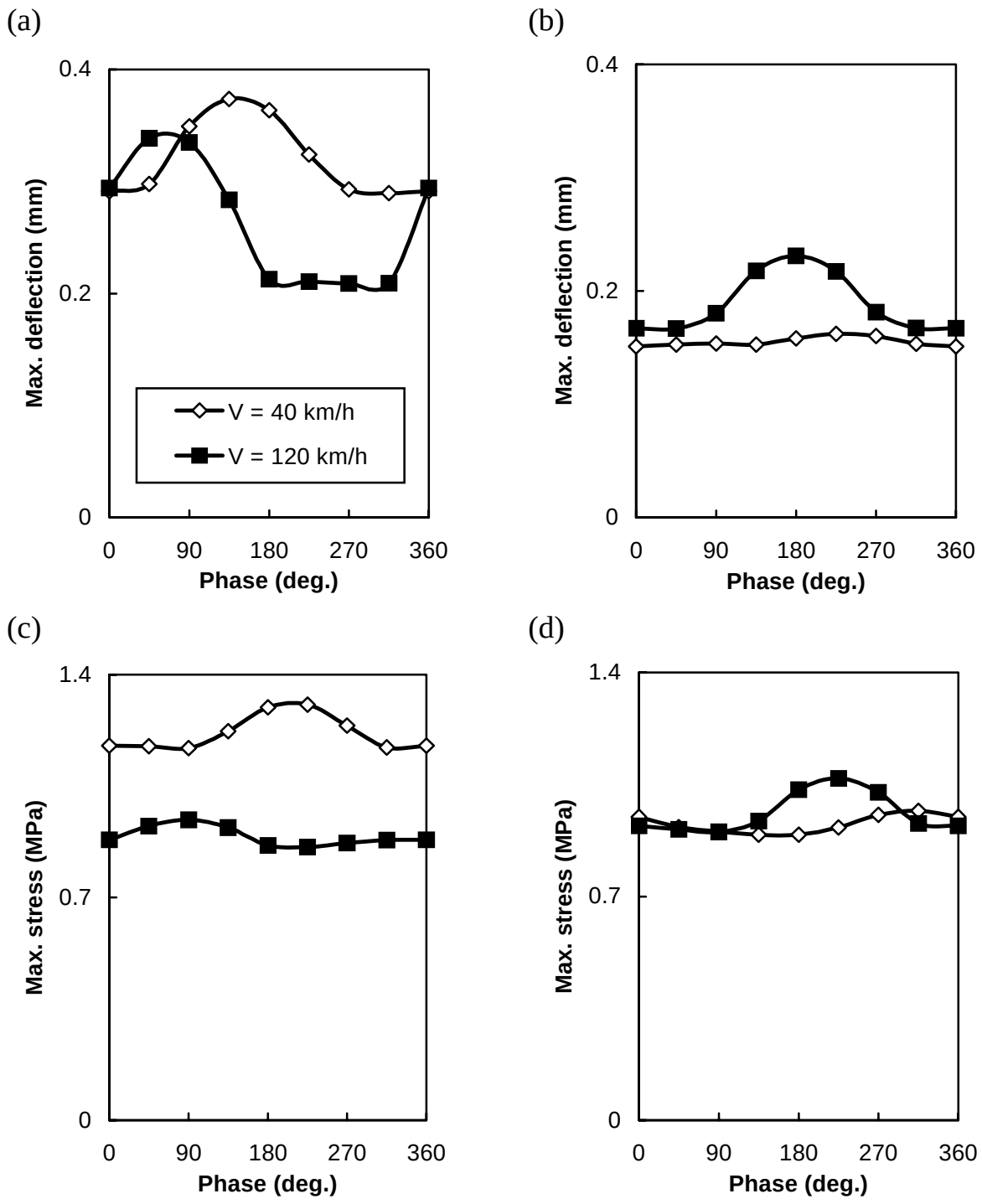

Figure 4.10. Effect of phase between front- and rear-axle loads: (a) on maximum deflection when frequency = 5 Hz; (b) when frequency = 15 Hz; (c) on maximum stress when frequency = 5 Hz; (d) when frequency = 15 Hz (1 MPa = 145 psi, 1 mm = 0.0394 in., 1 km/h = 0.63 mph)

3.4 SUMMARY

This report has investigated the dynamic displacement and stress responses of flexible pavements under moving loads of constant amplitude and harmonic and arbitrary variations. The flexible pavement has been modeled using a plate of infinite extent on a viscoelastic foundation. We have developed formulations in the transformed field domains of time, space, and moving space, as explained in Chapter 2. From the developed formulations, extensive parametric studies could be conducted. The results of our analysis point to the following conclusions:

- The pavement responses under moving dual-wheel and dual-wheel single-axle loads of constant amplitude are almost the same. The dual-wheel tandem-axle loads, however, yield larger maximum deflections and slightly smaller or almost equal maximum stresses depending on the presence of viscous damping.
- For the moving tandem-axle loads of constant amplitude, the following results were shown:
  - Without viscous damping, the response is symmetric with respect to the center of the tandem-axle loads, and the maximum deflection and stress increase slightly with increasing velocity. With viscous damping, the response is no longer symmetric, the maximum deflection occurs under the rear-axle loads, and the maximum deflection and stress decrease with increasing velocity.
  - The maximum deflection and stress decrease as the viscous damping value or foundation stiffness increase. Therefore, a stiffer foundation can reduce rutting and cracking.
  - The maximum deflection decreases and the maximum stress increases as the elastic modulus of the surface layer increases.
- For the moving tandem-axle loads of arbitrary variation caused by pavement surface roughness, the maximum load amplitude and corresponding deflection and stress increase significantly compared to those obtained with the ideally smooth pavement.
- For the moving tandem-axle loads of harmonic variation, the following results were shown:
  - Without viscous damping, the maximum deflection and stress increase with increasing load frequency and the phase between the front- and rear-axle loads make the maximum deflection smaller but the maximum stress larger.
  - With viscous damping, the maximum deflection and stress decrease with increasing frequency for a low velocity, but the initial increase in the maximum deflection and stress can be observed within low frequencies for a high velocity. The maximum deflection and stress increase initially and decrease again with increasing velocity for a low frequency, but for a high frequency, they tend to increase with increasing velocity.
  - The phase between the front- and rear-axle loads can make the maximum deflection and stress significantly larger. Because the phase effect cannot be considered with single-axle loads, the use of tandem-axle loads is necessary to find the accurate pavement stresses.

CHAPTER 5. INTEGRATING THE EFFECT OF MOVING TANDEM-AXLE LOADS INTO THE CRCP-10 COMPUTER PROGRAM

5.1 WHEEL LOAD STRESS CALCULATION IN PREVIOUS CRCP PROGRAMS

In the previous CRCP computer programs, including CRCP-8 (Ref 11) and CRCP-9 (Refs 8, 9, 10), the stresses caused by wheel load applications are calculated using Westergaard equations considering a single wheel load in the interior of a slab (Ref 1). If the external load is applied to any finite element node, this load will act as a line load because the finite element model developed for CRCP-9 is two dimensional. Therefore, the stresses caused by wheel loads have been obtained using Westergaard equations by

$$\sigma = \frac{3(1+\nu)P}{2\pi h^2}(\ln\frac{l}{b} + 0.6159)\ , \tag{5.1}$$

where h is the thickness of the slab in inches, ν is Poisson's ratio, and P is the magnitude of the load in pounds. The radius of relative stiffness l is defined by

$$l = \left[\frac{Eh^3}{12(1-\nu^2)k}\right]^{0.25}, \tag{5.2}$$

where E is the modulus of elasticity and k is the modulus of subgrade reaction. In Eq. 5.1, b is defined by

$$b = a \qquad \text{when} \quad a \geq 1.724h \tag{5.3}$$

$$b = \sqrt{1.6a^2 + h^2} - 0.675h \qquad \text{when} \quad a < 1.724h\,, \tag{5.4}$$

where a is the radius of the circular loaded area.

The stresses caused by the environmental loads are calculated by using the finite element model, the stresses caused by the external wheel loads are calculated by the above Westergaard equations, and those stresses are added to yield the concrete stresses that result from the combined effects in the slab. With this approach, the effect of multiple wheel loads such as dual tires, single axles, and tandem axles is ignored. Moreover, because the stress obtained using the above equations is static, the effect of the dynamic variation of the moving load is also ignored.

5.2 WHEEL LOAD STRESS CALCULATION IN CRCP-10

In order to include the effects of multiple wheel loads and dynamic variation of the moving loads, we have used the formulations explained in Chapter 2 to obtain critical wheel load stresses in the concrete pavement systems. The final critical tensile stresses can be obtained by comparing three different stresses including wheel load stresses obtained from the formulations developed in this study; environmental load stresses obtained from the finite element model; and the combined stresses, obtained by adding wheel load and environmental load stresses. Because the wheel load stresses do not always exist, the critical stresses may be only the environmental stresses or the combined stresses of wheel loads and environmental loads. Figure 5.1 shows the methodology to find the critical stress distributions through the depth of the concrete slab. In the examples shown in the figure, the critical stresses of the upper half of the concrete slab are the stresses induced by the environmental loads because the wheel loads induce compressive stresses in the upper half of the slab. On the other hand, the combined stresses of environmental load and wheel load stresses are the critical stresses through the lower half of the concrete slab because the wheel loads induce tensile stresses in the lower half of the slab. We also found that the maximum tensile stress can occur at the bottom, not always at the surface, and can occur when the temperature increases, not always when the temperature drops. In this case, a new crack will be initiated from the bottom.

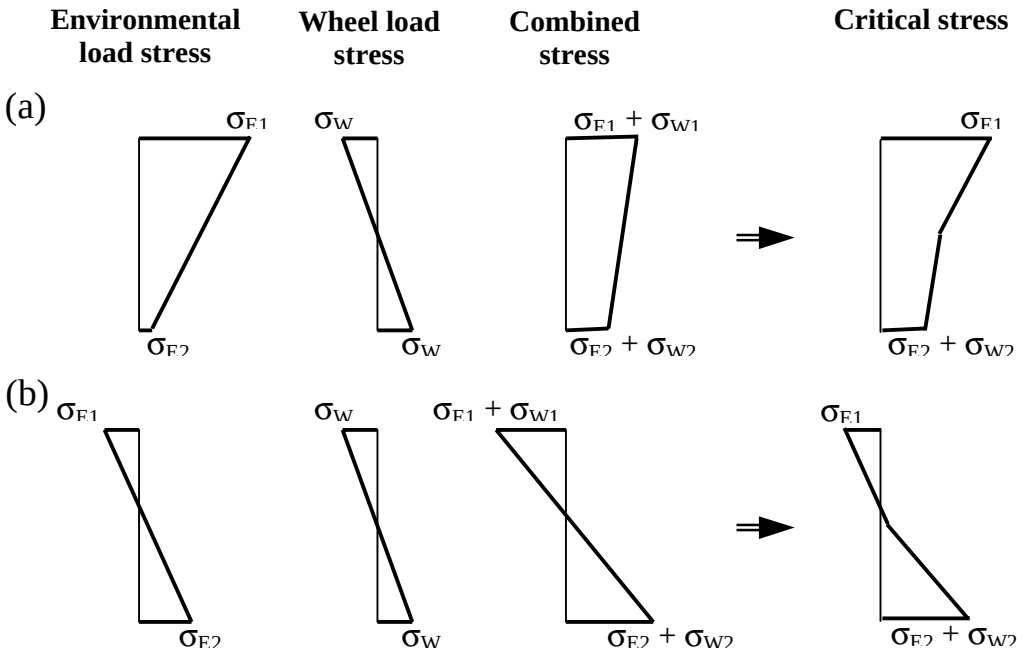

Figure 5.1. Critical stress distribution through depth: (a) when temperature drops and maximum tensile stress occurs at surface; (b) when temperature increases and maximum tensile stress occurs at bottom

The input screen in CRCP-10 for the wheel load stress calculation is shown in Figure 5.2. Users can select one of two different options for the wheel load calculation: One is to consider the single static wheel load, which is the same input in CRCP-9; the other considers the moving dynamic tandem-axle loads. For load geometry, the needed input variables include center-to-center distance between dual tires, distance between axles, center-to-center distance between left and right wheels, and loaded lengths of the tire print in the longitudinal and transverse directions. For the time history of the load variation, two kinds of moving loads can be defined. One is the moving load of constant amplitude, and the other is the moving load of harmonic variation. For the moving load of constant amplitude, it is assumed that the load amplitude is constant when the load is moving. For the moving load of harmonic variation, it is assumed that the load amplitude changes with time. Figure 5.3 shows the definitions of the input variables for the load time history. In the input screen (Figure 5.2), the average single-axle load is *A* in Figure 5.3, the half amplitude is *B*, the load frequency is *f*, and the phase angle is θ. Other input variables include vehicle speed, viscous damping coefficient of underlying layers, and linear hysteretic damping of underlying layers. The effects of these input variables have been investigated in Chapters 3 and 4. The subroutine program to calculate critical stresses under the moving dynamic tandem-axle loads is listed in Appendix A.

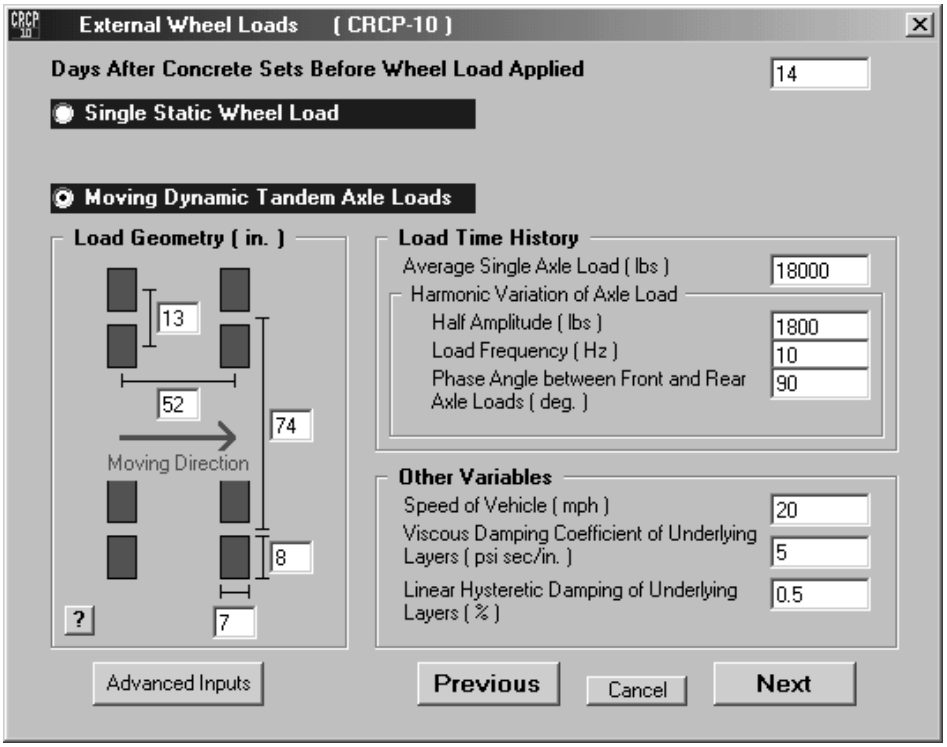

Figure 5.2. Input screen to define moving tandem-axle loads

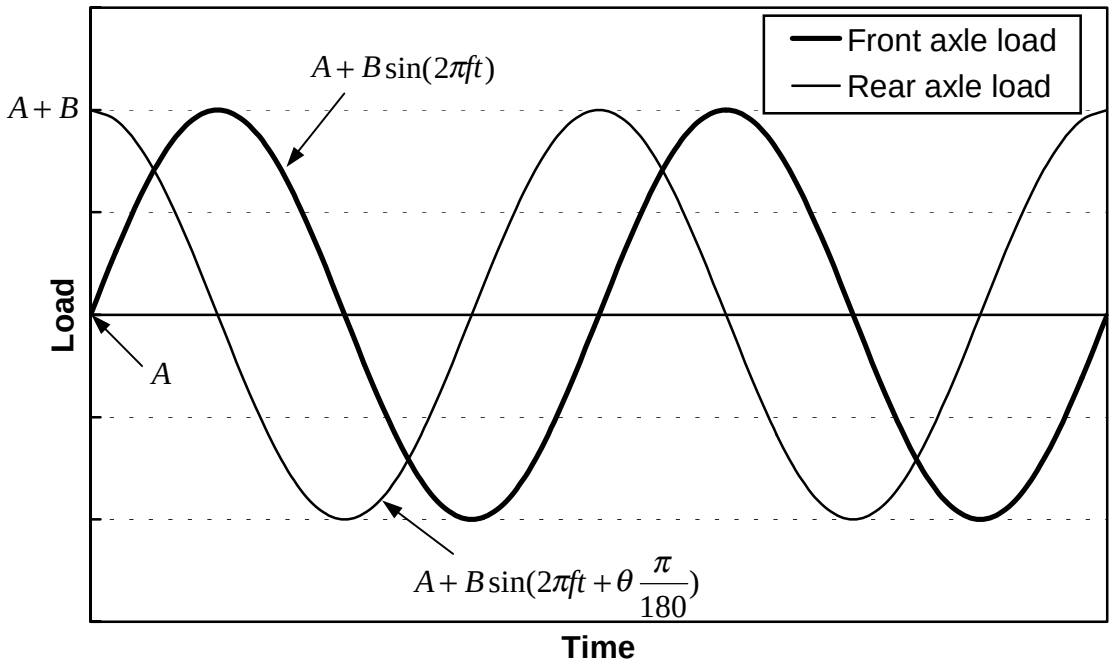

Figure 5.3. Definition of load time history

CHAPTER 6. SUMMARY, CONCLUSIONS, AND RECOMMENDATIONS

6.1 SUMMARY

This report has investigated the dynamic displacement and stress responses of rigid and flexible pavements subjected to moving tandem-axle loads of constant amplitude and harmonic and arbitrary variations. The pavement systems have been modeled using a plate of infinite extent on a viscoelastic foundation. We have developed formulations in the transformed field domain using the following: (1) a double Fourier transform in space and moving space for moving loads of constant amplitude; (2) a triple Fourier transform in time, space, and moving space for moving loads of arbitrary variation; and (3) a double Fourier transform in space and moving space for the steady-state response to moving harmonic loads. The effects of viscous damping, vehicle speed, load frequency, and phase between front and rear axle loads on the maximum deflection and stress have been investigated. The deflection and stress distributions near the loads have also been analyzed. The results of our analysis of viscoelasticity show significant differences from those obtained with an elastic system. The pavement surface roughness causes dynamic variations in the load amplitude, and the maximum deflection and stress can significantly increase accordingly. The variation in the load amplitude and the differences in the phase angles between front- and rear-axle loads can make the maximum deflection and stress considerably larger. The use of tandem-axle loads is necessary to find the accurate responses because the phase effect cannot be considered with single axle loads. The formulations developed to find the wheel load stresses that result from the moving tandem-axle loads have been integrated into CRCP-10, which is the updated computer program of CRCP-9.

6.2 CONCLUSIONS

This study was conducted to develop formulations for the pavement stress calculation under the moving tandem-axle loads and to investigate rigid and flexible pavement responses to those loads. It points to the following conclusions:

1. By using the developed formulations in the transformed field domain, one can efficiently obtain the pavement deflection and stress under the moving dynamic tandem-axle loads.
2. For the moving tandem-axle loads of constant amplitude we found the following: (1) without viscous damping, the displacement and stress distributions are symmetric with respect to the midpoint of the tandem-axle loads, and the maximum deflection and stress remain almost the same regardless of velocity; and (2) with viscous damping, the displacement and stress distributions are no longer symmetric; the maximum deflection and stress initially increase slightly and then decrease with increasing velocity; and the maximum deflection and stress occur under the rear-axle loads.

3. For the moving tandem-axle loads of arbitrary variation caused by pavement surface roughness, the maximum load amplitude and corresponding deflection and stress increase significantly compared to those obtained with the ideally smooth pavement.
4. For the moving tandem-axle loads of harmonic variation we found the following: (1) without viscous damping, the maximum stress is not much affected by the load frequency for concrete pavements; the maximum deflection and stress increase with increasing load frequency, and the phase between the front- and rear-axle loads makes the maximum deflection smaller but the maximum stress larger for flexible pavements; (2) with viscous damping, the displacement and stress distributions are affected significantly by the load frequency, and the maximum deflection and stress tend to decrease as the load frequency increases; and (3) the phase between front- and rear-axle loads can make the maximum deflection and stress significantly larger. Because the phase effect cannot be considered with single-axle loads, the use of tandem-axle loads to find the accurate pavement stresses is necessary.
5. The CRCP-10 computer program includes the effect of the moving dynamic tandem-axle loads.

6.3 RECOMMENDATIONS

The above summary and conclusions clearly indicate the significant effects pavement roughness has on wheel load deflections and stresses, and on the subsequent rutting and fatigue life of pavement systems. The current practice of analysis using static loads will underestimate the maximum wheel load deflections and stresses, and the resulting pavement design will be less conservative. Considering ever-increasing public pressure to provide optimal pavement systems with limited resources, it is important to estimate wheel load deflections and stresses and the resulting pavement remaining lives accurately for input into pavement management systems. Further research is needed in this area to identify characteristics of pavement systems and truck configurations that have an effect on dynamic responses of pavement systems. In addition, to improve the accuracy of the CRCP-10 computer program, the calibration of the program with field data should be further performed to obtain more reasonable ranges of input values and analysis results. Because the wheel load stress calculation procedure included in the program ignores discontinuities at cracks, joints, and edges of the pavement, further research is needed to find their effects.

REFERENCES

1. Westergaard, H. M. "Stresses in Concrete Pavements Computed by Theoretical Analysis." *Public Roads*, Vol. 7, 1925, pp. 25-35.
2. Huang, Y. H. *Pavement Analysis and Design*. Prentice Hall, New Jersey, 1993.
3. Zaghloul, S. M., and T. D. White. "Use of a Three Dimensional Dynamic Finite Element Program for Analysis of Flexible Pavement." *Transportation Research Record 1388*, TRB, National Research Council, Washington, D.C., 1993, pp. 60-69.
4. Zaghloul, S. M., and T. D. White. "Non-Linear Dynamic Analysis of Concrete Pavements." *Proceedings of the Fifth International Conference on Concrete Pavement Design and Rehabilitation*, West Lafayette, Indiana, 1993, pp. 277-292.
5. Zaman, M., M. Taheri, and A. Alvappillai. "Dynamic Response of a Thick Plate on Viscoelastic Foundation to Moving Loads." *International Journal for Numerical and Analytical Methods in Geomechanics*, Vol. 15, 1991, pp. 627-647.
6. Liu, C., B. F. McCullough, and H. S. Oey. "Response of Rigid Pavements Due to Vehicle-Road Interaction." *Journal of Transportation Engineering*, ASCE, Vol. 126, No. 3, 2000, pp. 237-242.
7. Kim, S. M., and J. M. Roesset. *Dynamic Response of Pavement Systems to Moving Loads*. Geotechnical Engineering Report GR97-4. Geotechnical Engineering Center, The University of Texas at Austin, 1997.
8. Kim, S. M., M. C. Won, and B. F. McCullough. "Development of CRCP-9 Computer Program for Analysis of CRC Pavements," *Proceedings of the 80th Annual Meeting of the Transportation Research Board*, TRB, National Research Council, Washington, D.C., 2001 (CD-ROM).
9. Kim, S. M., M. C. Won, and B. F. McCullough. *CRCP-9: Improved Computer Program for Mechanistic Analysis of Continuously Reinforced Concrete Pavements.* Report 1831-2. Center for Transportation Research, The University of Texas at Austin, 2001.
10. Kim, S. M., M. C. Won, and B. F. McCullough. *CRCP-9 Computer Program User's Guide*. Report 1831-3. Center for Transportation Research, The University of Texas at Austin, 2001.
11. Won, M. C., T. Dossey, S. Easley, and J. Speer. *CRCP-8 Program User's Guide*. Center for Transportation Research, The University of Texas at Austin, 1995.

12. Foinquinos, R., and J. M. Roesset. *Dynamic Nondestructive Testing of Pavements*. Geotechnical Engineering Report GR95-4. Geotechnical Engineering Center, The University of Texas at Austin, 1995.

13. Kim, S. M., and J. M. Roesset. "Moving Loads on a Plate on Elastic Foundation." *Journal of Engineering Mechanics*, ASCE, Vol. 124, No. 9, 1998, pp. 1010-1016.

14. Kausel, E., and J. M. Roesset. "Frequency Domain Analysis of Undamped Systems." *Journal of Engineering Mechanics*, ASCE, Vol. 118, No. 4, 1992, pp. 721-732.

15. *Structural Dynamic Simulation for MLS, Computer Program*, Center for Transportation Research, The University of Texas at Austin, 1992.

16. Kim, S. M., J. M. Roesset, T. D. White, and F. Hugo. *Dimensional Analysis of the Mobile Load Simulator Action on Pavements*. Report 2914-1F. Center for Transportation Research, The University of Texas at Austin, 1995.

APPENDIX A:

LIST OF SUBROUTINE PROGRAM WHEELMV

```
C*******************************************************************************
      SUBROUTINE WHEELMV(H,E,POI,AK,WEIGHT,DX,DY,
     +           DISTIRE,DISWH,DISAX,DEGREE,VEL,PAMP,PAMPH,OMHZ,VDAMP,
     +           HDAMP,WHSTR)
C
C     THIS SUBROUTINE IS USED TO ANALYZE LONGITUDINAL STRESS RESPONSE
C     FOR A PLATE ON VISCOELASTIC FOUNDATION WITH INFINITE LENGTH DUE
C     TO THE MOVING TANDEM (TWO AXLE) LOADS WITH CONSTANT AND HARMONIC
C     VARIATIONS.
C     INSTEAD OF SUPERPOSITION, DIFFERENT LOAD GEOMETRIES ARE USED.
C     ONLY IFT IS USED FOR SPACE AND MOVING SPACE.
C
      IMPLICIT REAL*8(A-H,O-Z)
      DIMENSION RESP(2050),REC(2050)
      DIMENSION SIG(1025,1025)
      COMPLEX*16 CRESP(1025),CREC(1025)
      COMPLEX*16 TRF,CFX,CFY,AK1,CTOT(1025,1025)
      EQUIVALENCE (CRESP(1),RESP(1)),(CREC(1),REC(1))
C
C      DX: TIRE CONTACT LENGTH IN X-DIRECTION
C      DY: TIRE CONTACT LENGTH IN Y-DIRECTION
C      VEL: LOAD VELOCITY
C      VDAMP: VISCOUS DAMPING COEFFICIENT (C VALUE)
C      HDAMP: MATERIAL DAMPING (LINEAR HYSTERETIC DAMPING) COEFFICIENT
C      E: ELASTIC MODULUS
C      H: THICKNESS
C      POI: POISSON'S RATIO
C      AK: STIFFNESS PER UNIT OF AREA
C      PAMP: TOTAL LOAD ON EACH TIRE PRINT AREA
C      PAMPH: PEAK HARMONIC LOAD ON EACH TIRE PRINT AREA
C      OMHZ: LOAD FREQUENCY (HZ)
C      DISTIRE: CENTER-TO-CENTER DISTANCE BETWEEN DUAL TIRES
C      DISWH: CENTER-TO-CENTER DISTANCE BETWEEN LEFT AND RIGHT TIRES
C      DISAX: CENTER-TO-CENTER DISTANCE BETWEEN AXLES
C      DEGREE: PHASE ANGLE (DEGREE) BETWEEN AXLES
C
C      AM: MASS DENSITY PER UNIT OF AREA
       AM=0.0000015*WEIGHT*H
C      DL: DELTA LENGTH (in.)
C      NPTRL: NO. OF TRANSFORMED POINTS
C      X0: X-COORDINATE OF THE CENTER OF REAR RIGHT OUTSIDE TIRE (in.)
       DL=1.0
       NPTRL=1024
       X0=500.
C
C      IF(OMHZ.EQ.0.) PAMPH=0.
       IF(PAMPH.EQ.0.) OMHZ=0.
       DD=E*H**3/(12.*(1.-POI**2))
       ALTOT=NPTRL*DL
       NPL2=NPTRL/2
       PI=DACOS(-1.D0)
       PI2=PI*2.D0
       DXI=PI2/ALTOT
       Y0=FLOAT(NPL2)*DL
       OMEGA=OMHZ*PI2
       PHSLD=DEGREE*PI/180.
       CONST=E*H/(-2.*(1.-POI*POI))
       VIS=VDAMP
       DO I=1,NPTRL+1
       DO J=1,NPTRL+1
          SIG(I,J)=0.
       ENDDO
       ENDDO
```

```
C
      DX2=DX/2.
      DY2=DY/2.
C
      INDEX=1
      IF(PAMPH.EQ.0.) INDEX=2
  123 CONTINUE
      IF(INDEX.EQ.1) THEN
        Q=PAMPH/(DX*DY)
      ELSE
        Q=PAMP/(DX*DY)
        OMEGA=0.
        PHSLD=0.
      ENDIF
C
      DO I=1,NPTRL+1
      CRESP(I)=0.
      CREC(I)=0.
      ENDDO
C
      DO 1000 KIM=1,NPL2
      IF(KIM.EQ.1) THEN
      AIX=0.001
      ELSE
      AIX=KIM-1
      ENDIF
      XIX=AIX*DXI
      XIX2=XIX*XIX
      CFX=(CDEXP((0.,1.)*XIX*DX2)-CDEXP(-(0.,1.)*XIX*DX2))/
     +    XIX*(-(0.,1.))*(CDEXP(-(0.,1.)*XIX*X0)+CDEXP(-(0.,1.)*XIX*
     +    (X0+DISAX))*CDEXP((0.,1.)*PHSLD))
C
      DO 31 MIN=1,NPL2
      IF(MIN.EQ.1) THEN
      AI=0.001
      ELSE
      AI=MIN-1
      ENDIF
      XIY=AI*DXI
      XIY2=XIY*XIY
       IF((OMEGA-VEL*XIX).LT.0.) AK1=AK*(1.-2.*(0.,1.)*HDAMP)
       IF((OMEGA-VEL*XIX).EQ.0.) AK1=AK
       IF((OMEGA-VEL*XIX).GT.0.) AK1=AK*(1.+2.*(0.,1.)*HDAMP)
      TRF=1./(AK1+DD*(XIX2+XIY2)**2-AM*(OMEGA-VEL*XIX)**2+VIS*(0.,1.)*
     +    (OMEGA-VEL*XIX))*(XIX2+POI*XIY2)
      CFY=-Q*(CDEXP((0.,1.)*XIY*DY2)-CDEXP(-(0.,1.)*XIY*DY2
     +    ))/XIY*(0.,1.)*(CDEXP(-(0.,1.)*XIY*Y0)+CDEXP(-(0.,1.)*XIY*
     +    (Y0+DISTIRE))+CDEXP(-(0.,1.)*XIY*(Y0+DISWH))+CDEXP(-(0.,1.)*
     +    XIY*(Y0+DISTIRE+DISWH)))
      CRESP(MIN)=CFY*TRF*DXI/PI2
C
       II=NPTRL+2-MIN
       IF(MIN.EQ.1) THEN
         AI=0.001
       ELSE
         AI=MIN-1
       ENDIF
      XIY=-AI*DXI
      XIY2=XIY*XIY
       IF((OMEGA-VEL*XIX).LT.0.) AK1=AK*(1.-2.*(0.,1.)*HDAMP)
       IF((OMEGA-VEL*XIX).EQ.0.) AK1=AK
       IF((OMEGA-VEL*XIX).GT.0.) AK1=AK*(1.+2.*(0.,1.)*HDAMP)
      TRF=1./(AK1+DD*(XIX2+XIY2)**2-AM*(OMEGA-VEL*XIX)**2+VIS*(0.,1.)*
```

```
     +    (OMEGA-VEL*XIX))*(XIX2+POI*XIY2)
      CFY=-Q*(CDEXP((0.,1.)*XIY*DY2)-CDEXP(-(0.,1.)*XIY*DY2
     +    ))/XIY*(0.,1.)*(CDEXP(-(0.,1.)*XIY*Y0)+CDEXP(-(0.,1.)*XIY*
     +    (Y0+DISTIRE))+CDEXP(-(0.,1.)*XIY*(Y0+DISWH))+CDEXP(-(0.,1.)*
     +    XIY*(Y0+DISTIRE+DISWH)))
      CRESP(II)=CFY*TRF*DXI/PI2
   31 CONTINUE
      CRESP(NPL2+1)=0.
      CALL FOUR2(RESP,NPTRL,1,1,1)
C
       DO I=1,NPTRL+1
          CTOT(KIM,I)=CRESP(I)*CFX*DXI/PI2*CONST
       ENDDO
C
       KIMM=NPTRL+2-KIM
       IF(KIM.EQ.1) THEN
         AIX=0.001
       ELSE
         AIX=KIM-1
       ENDIF
      XIX=-AIX*DXI
      XIX2=XIX*XIX
      CFX=(CDEXP((0.,1.)*XIX*DX2)-CDEXP(-(0.,1.)*XIX*DX2))/
     +    XIX*(-(0.,1.))*(CDEXP(-(0.,1.)*XIX*X0)+CDEXP(-(0.,1.)*XIX*
     +    (X0+DISAX))*CDEXP((0.,1.)*PHSLD))
C
      DO 32 MIN=1,NPL2
      IF(MIN.EQ.1) THEN
      AI=0.001
      ELSE
      AI=MIN-1
      ENDIF
      XIY=AI*DXI
      XIY2=XIY*XIY
       IF((OMEGA-VEL*XIX).LT.0.) AK1=AK*(1.-2.*(0.,1.)*HDAMP)
       IF((OMEGA-VEL*XIX).EQ.0.) AK1=AK
       IF((OMEGA-VEL*XIX).GT.0.) AK1=AK*(1.+2.*(0.,1.)*HDAMP)
      TRF=1./(AK1+DD*(XIX2+XIY2)**2-AM*(OMEGA-VEL*XIX)**2+VIS*(0.,1.)*
     +    (OMEGA-VEL*XIX))*(XIX2+POI*XIY2)
      CFY=-Q*(CDEXP((0.,1.)*XIY*DY2)-CDEXP(-(0.,1.)*XIY*DY2
     +    ))/XIY*(0.,1.)*(CDEXP(-(0.,1.)*XIY*Y0)+CDEXP(-(0.,1.)*XIY*
     +    (Y0+DISTIRE))+CDEXP(-(0.,1.)*XIY*(Y0+DISWH))+CDEXP(-(0.,1.)*
     +    XIY*(Y0+DISTIRE+DISWH)))
      CRESP(MIN)=CFY*TRF*DXI/PI2
C
       II=NPTRL+2-MIN
       IF(MIN.EQ.1) THEN
         AI=0.001
       ELSE
         AI=MIN-1
       ENDIF
      XIY=-AI*DXI
      XIY2=XIY*XIY
       IF((OMEGA-VEL*XIX).LT.0.) AK1=AK*(1.-2.*(0.,1.)*HDAMP)
       IF((OMEGA-VEL*XIX).EQ.0.) AK1=AK
       IF((OMEGA-VEL*XIX).GT.0.) AK1=AK*(1.+2.*(0.,1.)*HDAMP)
      TRF=1./(AK1+DD*(XIX2+XIY2)**2-AM*(OMEGA-VEL*XIX)**2+VIS*(0.,1.)*
     +    (OMEGA-VEL*XIX))*(XIX2+POI*XIY2)
      CFY=-Q*(CDEXP((0.,1.)*XIY*DY2)-CDEXP(-(0.,1.)*XIY*DY2
     +    ))/XIY*(0.,1.)*(CDEXP(-(0.,1.)*XIY*Y0)+CDEXP(-(0.,1.)*XIY*
     +    (Y0+DISTIRE))+CDEXP(-(0.,1.)*XIY*(Y0+DISWH))+CDEXP(-(0.,1.)*
     +    XIY*(Y0+DISTIRE+DISWH)))
      CRESP(II)=CFY*TRF*DXI/PI2
```

```
   32 CONTINUE
      CRESP(NPL2+1)=0.
      CALL FOUR2(RESP,NPTRL,1,1,1)
C
       DO I=1,NPTRL+1
          CTOT(KIMM,I)=CRESP(I)*CFX*DXI/PI2*CONST
       ENDDO
 1000 CONTINUE
C
       DO I=1,NPTRL+1
          CTOT(NPL2+1,I)=0.
       ENDDO
C
       DO J=1,NPTRL+1
          DO I=1,NPTRL+1
             CREC(I)=CTOT(I,J)
          ENDDO
C
          CALL FOUR2(REC,NPTRL,1,1,1)
C
          DO I=1,NPTRL+1
             CTOT(I,J)=CREC(I)
          ENDDO
       ENDDO
C
       NDISWH=DISWH/DL
       NDISTIRE=DISTIRE/DL
       NDISWT=NDISWH+NDISTIRE
       NDISWT2=NDISWT/2
C
       AMAX=0.
       DO I=1,NPTRL+1
          DO J=1,NPL2+1+NDISWT2
               IF(index.NE.1) THEN
                  SIG(I,J)=SIG(I,J)+REAL(CTOT(I,J))
             IF(SIG(I,J).GT.AMAX) THEN
                  AMAX=SIG(I,J)
               IAMAX=I
               JAMAX=J
             ENDIF
               ELSE
                  SIG(I,J)=CDABS(CTOT(I,J))
               ENDIF
          ENDDO
       ENDDO
C
       IF(INDEX.EQ.1) then
         INDEX=2
         GO TO 123
       ENDIF
C
       WHSTR=AMAX
C
       RETURN
       END
C*******************************************************************************
C     ------------------------------------------------------------------------
      SUBROUTINE FOUR2 (DATA,N,NDIM,ISIGN,IFORM)
      IMPLICIT REAL*8(A-H,O-Z),INTEGER*4(I-N)
      DIMENSION DATA(1), N(1)
      NTOT=1
      DO 10 IDIM=1,NDIM
 10   NTOT=NTOT*N(IDIM)
```

```
      IF (IFORM) 70,20,20
 20   NREM=NTOT
      DO 60 IDIM=1,NDIM
      NREM=NREM/N(IDIM)
      NPREV=NTOT/(N(IDIM)*NREM)
      NCURR=N(IDIM)
      IF (IDIM-1+IFORM) 30,30,40
 30   NCURR=NCURR/2
 40   CALL BITRV (DATA,NPREV,NCURR,NREM)
      CALL COOL2 (DATA,NPREV,NCURR,NREM,ISIGN)
      IF (IDIM-1+IFORM) 50,50,60
 50   CALL FIXRL (DATA,N(1),NREM,ISIGN,IFORM)
      NTOT=(NTOT/N(1))*(N(1)/2+1)
 60   CONTINUE
      RETURN
 70   NTOT=(NTOT/N(1))*(N(1)/2+1)
      NREM=1
      DO 100 JDIM=1,NDIM
      IDIM=NDIM+1-JDIM
      NCURR=N(IDIM)
      IF (IDIM-1) 80,80,90
 80   NCURR=NCURR/2
      CALL FIXRL (DATA,N(1),NREM,ISIGN,IFORM)
      NTOT=NTOT/(N(1)/2+1)*N(1)
 90   NPREV=NTOT/(N(IDIM)*NREM)
      CALL BITRV (DATA,NPREV,NCURR,NREM)
      CALL COOL2 (DATA,NPREV,NCURR,NREM,ISIGN)
 100  NREM=NREM*N(IDIM)
      RETURN
      END
C     ------------------------------------------------------------------------------
C     ------------------------------------------------------------------------------
      SUBROUTINE BITRV (DATA,NPREV,N,NREM)
      IMPLICIT REAL*8(A-H,O-Z),INTEGER*4(I-N)
C     SHUFFLE THE DATA BY 'BIT REVERSAL'.
C     DIMENSION DATA(NPREV,N,NREM)
C     DATA(I1,I2REV,I3) = DATA(I1,I2,I3), FOR ALL I1 FROM 1 TO NPREV,
C     ALL I2 FROM 1 TO N (WHICH MUST BE A POWER OF TWO), AND ALL I3
C     FROM 1 TO NREM, WHERE I2REV-1 IS THE BITWISE REVERSAL OF I2-1.
C     FOR EXAMPLE, N = 32, I2-1 = 10011 AND I2REV-1 = 11001.
      DIMENSION DATA(1)
      IP0=2
      IP1=IP0*NPREV
      IP4=IP1*N
      IP5=IP4*NREM
      I4REV=1
      DO 60 I4=1,IP4,IP1
      IF (I4-I4REV) 10,30,30
 10   I1MAX=I4+IP1-IP0
      DO 20 I1=I4,I1MAX,IP0
      DO 20 I5=I1,IP5,IP4
      I5REV=I4REV+I5-I4
      TEMPR=DATA(I5)
      TEMPI=DATA(I5+1)
      DATA(I5)=DATA(I5REV)
      DATA(I5+1)=DATA(I5REV+1)
      DATA(I5REV)=TEMPR
 20   DATA(I5REV+1)=TEMPI
 30   IP2=IP4/2
 40   IF (I4REV-IP2) 60,60,50
 50   I4REV=I4REV-IP2
      IP2=IP2/2
      IF (IP2-IP1) 60,40,40
```

```
 60   I4REV=I4REV+IP2
      RETURN
      END
C     ------------------------------------------------------------------------
C     ------------------------------------------------------------------------
      SUBROUTINE COOL2 (DATA,NPREV,N,NREM,ISIGN)
      IMPLICIT REAL*8(A-H,O-Z),INTEGER*4(I-N)
C     FOURIER TRANSFORM OF LENGTH N BY THE COOLEY-TUKEY ALGORITHM.
C     BIT-REVERSED TO NORMAL ORDER.
C     DIMENSION DATA(NPREV,N,NREM)
C     COMPLEX DATA
C     DATA(I1,J2,I3) = SUM(DATA(I1,I2,I3)*EXP(ISIGN*2*PI*I*((I2-1)*
C     (J2-1)/N))), SUMMED OVER I2 = 1 TO N FOR ALL I1 FROM 1 TO NPREV,
C     J2 FROM 1 TO N AND I3 FROM 1 TO NREM.  N MUST BE A POWER OF TWO.
C     FACTORING N BY FOURS SAVES ABOUT TWENTY FIVE PERCENT OVER FACTOR-
C     ING BY TWOS.
C     NOTE--IT IS NOT NECESSARY TO REWRITE THIS SUBROUTINE INTO COMPLEX
C     NOTATION SO LONG AS THE FORTRAN COMPILER USED STORES REAL AND
C     IMAGINARY PARTS IN ADJACENT STORAGE LOCATIONS.  IT MUST ALSO
C     STORE ARRAYS WITH THE FIRST SUBSCRIPT INCREASING FASTEST.
      DIMENSION DATA(1)
      TWOPI=2.*(4.*DATAN(1.D0))*ISIGN
      IP0=2
      IP1=IP0*NPREV
      IP4=IP1*N
      IP5=IP4*NREM
      IP2=IP1
      NPART=N
 10   IF (NPART-2) 50,30,20
 20   NPART=NPART/4
      GO TO 10
C     DO A FOURIER TRANSFORM OF LENGTH TWO
 30   IP3=IP2*2
      DO 40 I1=1,IP1,IP0
      DO 40 I5=I1,IP5,IP3
      J0=I5
      J1=J0+IP2
      TEMPR=DATA(J1)
      TEMPI=DATA(J1+1)
      DATA(J1)=DATA(J0)-TEMPR
      DATA(J1+1)=DATA(J0+1)-TEMPI
      DATA(J0)=DATA(J0)+TEMPR
 40   DATA(J0+1)=DATA(J0+1)+TEMPI
      GO TO 140
C     DO A FOURIER TRANSFORM OF LENGTH FOUR (FROM BIT REVERSED ORDER)
 50   IP3=IP2*4
      THETA=TWOPI/     (IP3/IP1)
      SINTH= DSIN(THETA/2.)
      WSTPR=-2.*SINTH*SINTH
C     COS(THETA)-1, FOR ACCURACY.
      WSTPI= DSIN(THETA)
      WR=1.
      WI=0.
      DO 130 I2=1,IP2,IP1
      IF (I2-1) 70,70,60
 60   W2R=WR*WR-WI*WI
      W2I=2.*WR*WI
      W3R=W2R*WR-W2I*WI
      W3I=W2R*WI+W2I*WR
 70   I1MAX=I2+IP1-IP0
      DO 120 I1=I2,I1MAX,IP0
      DO 120 I5=I1,IP5,IP3
      J0=I5
```

```
      J1=J0+IP2
      J2=J1+IP2
      J3=J2+IP2
      IF (I2-1) 90,90,80
C     APPLY THE PHASE SHIFT FACTORS
 80   TEMPR=DATA(J1)
      DATA(J1)=W2R*TEMPR-W2I*DATA(J1+1)
      DATA(J1+1)=W2R*DATA(J1+1)+W2I*TEMPR
      TEMPR=DATA(J2)
      DATA(J2)=WR*TEMPR-WI*DATA(J2+1)
      DATA(J2+1)=WR*DATA(J2+1)+WI*TEMPR
      TEMPR=DATA(J3)
      DATA(J3)=W3R*TEMPR-W3I*DATA(J3+1)
      DATA(J3+1)=W3R*DATA(J3+1)+W3I*TEMPR
 90   T0R=DATA(J0)+DATA(J1)
      T0I=DATA(J0+1)+DATA(J1+1)
      T1R=DATA(J0)-DATA(J1)
      T1I=DATA(J0+1)-DATA(J1+1)
      T2R=DATA(J2)+DATA(J3)
      T2I=DATA(J2+1)+DATA(J3+1)
      T3R=DATA(J2)-DATA(J3)
      T3I=DATA(J2+1)-DATA(J3+1)
      DATA(J0)=T0R+T2R
      DATA(J0+1)=T0I+T2I
      DATA(J2)=T0R-T2R
      DATA(J2+1)=T0I-T2I
      IF (ISIGN) 100,100,110
 100  T3R=-T3R
      T3I=-T3I
 110  DATA(J1)=T1R-T3I
      DATA(J1+1)=T1I+T3R
      DATA(J3)=T1R+T3I
 120  DATA(J3+1)=T1I-T3R
      TEMPR=WR
      WR=WSTPR*TEMPR-WSTPI*WI+TEMPR
 130  WI=WSTPR*WI+WSTPI*TEMPR+WI
 140  IP2=IP3
      IF (IP3-IP4) 50,150,150
 150  RETURN
      END
C     ------------------------------------------------------------------------
C     ------------------------------------------------------------------------
      SUBROUTINE FIXRL (DATA,N,NREM,ISIGN,IFORM)
      IMPLICIT REAL*8(A-H,O-Z),INTEGER*4(I-N)
C     FOR IFORM = 0, CONVERT THE TRANSFORM OF A DOUBLED-UP REAL ARRAY,
C     CONSIDERED COMPLEX, INTO ITS TRUE TRANSFORM.  SUPPLY ONLY THE
C     FIRST HALF OF THE COMPLEX TRANSFORM, AS THE SECOND HALF HAS
C     CONJUGATE SYMMETRY.  FOR IFORM = -1, CONVERT THE FIRST HALF
C     OF THE TRUE TRANSFORM INTO THE TRANSFORM OF A DOUBLED-UP REAL
C     ARRAY.  N MUST BE EVEN.
C     USING COMPLEX NOTATION AND SUBSCRIPTS STARTING AT ZERO, THE
C     TRANSFORMATION IS--
C     DIMENSION DATA(N,NREM)
C     ZSTP = EXP(ISIGN*2*PI*I/N)
C     DO 10 I2=0,NREM-1
C     DATA(0,I2) = CONJ(DATA(0,I2))*(1+I)
C     DO 10 I1=1,N/4
C     Z = (1+(2*IFORM+1)*I*ZSTP**I1)/2
C     I1CNJ = N/2-I1
C     DIF = DATA(I1,I2)-CONJ(DATA(I1CNJ,I2))
C     TEMP = Z*DIF
C     DATA(I1,I2) = (DATA(I1,I2)-TEMP)*(1-IFORM)
C 10  DATA(I1CNJ,I2) = (DATA(I1CNJ,I2)+CONJ(TEMP))*(1-IFORM)
```

```
C     IF I1=I1CNJ, THE CALCULATION FOR THAT VALUE COLLAPSES INTO
C     A SIMPLE CONJUGATION OF DATA(I1,I2).
      DIMENSION DATA(1)
      TWOPI=2.*(4.*DATAN(1.D0))*ISIGN
      IP0=2
      IP1=IP0*(N/2)
      IP2=IP1*NREM
      IF (IFORM) 10,70,70
C     PACK THE REAL INPUT VALUES (TWO PER COLUMN)
 10   J1=IP1+1
      III2=2
      DATA(III2)=DATA(J1)
      IF (NREM-1) 70,70,20
 20   J1=J1+IP0
      I2MIN=IP1+1
      DO 60 I2=I2MIN,IP2,IP1
      DATA(I2)=DATA(J1)
      J1=J1+IP0
      IF (N-2) 50,50,30
 30   I1MIN=I2+IP0
      I1MAX=I2+IP1-IP0
      DO 40 I1=I1MIN,I1MAX,IP0
      DATA(I1)=DATA(J1)
      DATA(I1+1)=DATA(J1+1)
 40   J1=J1+IP0
 50   DATA(I2+1)=DATA(J1)
 60   J1=J1+IP0
 70   DO 80 I2=1,IP2,IP1
      TEMPR=DATA(I2)
      DATA(I2)=DATA(I2)+DATA(I2+1)
 80   DATA(I2+1)=TEMPR-DATA(I2+1)
      IF (N-2) 200,200,90
 90   THETA=TWOPI/FLOAT(N)
      SINTH= DSIN(THETA/2.)
      ZSTPR=-2.*SINTH*SINTH
      ZSTPI= DSIN(THETA)
      ZR=(1.-ZSTPI)/2.
      ZI=(1.+ZSTPR)/2.
      IF (IFORM) 100,110,110
 100  ZR=1.-ZR
      ZI=-ZI
 110  I1MIN=IP0+1
      I1MAX=IP0*(N/4)+1
      DO 190 I1=I1MIN,I1MAX,IP0
      DO 180 I2=I1,IP2,IP1
      I2CNJ=IP0*(N/2+1)-2*I1+I2
      IF (I2-I2CNJ) 150,120,120
 120  IF (ISIGN*(2*IFORM+1)) 130,140,140
 130  DATA(I2+1)=-DATA(I2+1)
 140  IF (IFORM) 170,180,180
 150  DIFR=DATA(I2)-DATA(I2CNJ)
      DIFI=DATA(I2+1)+DATA(I2CNJ+1)
      TEMPR=DIFR*ZR-DIFI*ZI
      TEMPI=DIFR*ZI+DIFI*ZR
      DATA(I2)=DATA(I2)-TEMPR
      DATA(I2+1)=DATA(I2+1)-TEMPI
      DATA(I2CNJ)=DATA(I2CNJ)+TEMPR
      DATA(I2CNJ+1)=DATA(I2CNJ+1)-TEMPI
      IF (IFORM) 160,180,180
 160  DATA(I2CNJ)=DATA(I2CNJ)+DATA(I2CNJ)
      DATA(I2CNJ+1)=DATA(I2CNJ+1)+DATA(I2CNJ+1)
 170  DATA(I2)=DATA(I2)+DATA(I2)
      DATA(I2+1)=DATA(I2+1)+DATA(I2+1)
```

```
 180  CONTINUE
      TEMPR=ZR-.5
      ZR=ZSTPR*TEMPR-ZSTPI*ZI+ZR
 190  ZI=ZSTPR*ZI+ZSTPI*TEMPR+ZI
C     RECURSION SAVES TIME, AT A SLIGHT LOSS IN ACCURACY.  IF AVAILABLE,
C     USE DOUBLE PRECISION TO COMPUTE ZR AND ZI.
 200  IF (IFORM) 270,210,210
C     UNPACK THE REAL TRANSFORM VALUES (TWO PER COLUMN)
 210  I2=IP2+1
      I1=I2
      J1=IP0*(N/2+1)*NREM+1
      GO TO 250
 220  DATA(J1)=DATA(I1)
      DATA(J1+1)=DATA(I1+1)
      I1=I1-IP0
      J1=J1-IP0
 230  IF (I2-I1) 220,240,240
 240  DATA(J1)=DATA(I1)
      DATA(J1+1)=0.
 250  I2=I2-IP1
      J1=J1-IP0
      DATA(J1)=DATA(I2+1)
      DATA(J1+1)=0.
      I1=I1-IP0
      J1=J1-IP0
      IF (I2-1) 260,260,230
  260 III2=2
      DATA(III2)=0.
 270  RETURN
      END
C*******************************************************************************
```